

THESIS ON NATURAL AND EXACT SCIENCES B77

**SEM study of selenization of different thin
metallic films**

OLGA VOLOBUJEVA

TALLINN 2008

TALLINN UNIVERSITY OF TECHNOLOGY
Faculty of Chemical and Materials Technology
Department of Materials Science

Dissertation was accepted for the defence of the degree of Doctor of Philosophy in Natural Sciences on June 17, 2008

Supervisor: Professor Enn Mellikov, Department of Material Science, Tallinn University of Technology, Tallinn, Estonia

Opponents: Professor Dieter Meissner, University of Wels, Austria
Professor Renate Hiesgen, Esslingen University of Applied Sciences, Germany

Defence of the thesis: August 12, 2008, at 13:00
Lecture hall: IV-103
Tallinn University of Technology, Ehitajate tee 5, Tallinn

Declaration: Hereby I declare that this doctoral thesis, my original investigation and achievement, submitted for the doctoral degree at Tallinn University of Technology has not been submitted for any academic degree.

Olga Volobujeva

Copyright: Olga Volobujeva, 2008
ISSN 1406-4774
ISBN 978-9985-59-831-3

LOODUS – JA TÄPPISTEADUSED B77

**Õhukeste metallikilede seleniseerimise
elektronmikroskoopiline uurimine**

OLGA VOLOBUJEVA

TALLINN 2008

TABLE OF CONTENT

INTRODUCTION.....	7
LIST OF PUBLICATIONS.....	9
1. LITERATURE OVERVIEW.....	12
1.1. Scanning Electron Microscopy.....	12
1.2. Methods of image formation (SE, BSE, EBSD).....	12
1.3. Analytical methods.....	14
1.4. Chalcopyrite materials for solar energy applications.....	15
1.5. The selenization of Cu-In layers.....	16
1.5.1. Introduction.....	16
1.5.2. Composition of precursor Cu-In layers at room temperature.....	17
1.5.3. Influence of thermal annealing to the composition of precursor Cu-In layers.....	19
1.5.4. Ex-situ investigation of selenization process of metal layers in elemental Se vapour.....	20
1.5.5. In-situ investigation of selenization process of metal layers in elemental Se vapour.....	23
1.5.6. Sulphurization of metallic films.....	26
1.6. Thermal annealing and selenization of electrochemically deposited films.....	27
1.6.1. Annealing electrodeposited films in Se non-containing atmospheres.....	28
1.6.2. Annealing of electrodeposited films in the Se containing atmosphere.....	29
1.7. Summary and goals of the research.....	31
2. EXPERIMENTAL.....	32
2.1. The deposition of precursor metallic films.....	32
2.1.1. The deposition of precursor copper–indium alloy films.....	32
2.1.2. The deposition of precursor copper–zinc-tin sequential films.....	32
2.1.3. Electrodeposition of CIS films.....	33
2.2. Selenization of metallic and electrochemically deposited CIS films.....	33
2.3. Methods of samples characterization.....	34
3. RESULTS AND DISCUSSION.....	37
3. 1. Selenization of Cu–In alloy films produced by co-sputtering of metals...37	
3.1.1. Precursor copper and indium alloy layers.....	37
3.1.2. Selenized copper and indium alloy layers.....	38
3.2. Selenization of Sn-Cu-Zn stacked layers.....	44
3.2.1. Sequential precursor films.....	45
3.2.2. Investigation of selenized Sn-Zn-Cu sequential films.....	47
3.3. Annealing of electrodeposited layers.....	51

3.3.1. Influence of annealing conditions on the structural quality of CuInSe ₂ thin films.....	51
4. CONCLUSIONS.....	57
REFERENCES.....	58
ABSTRACT.....	67
KOKKUVÕTE.....	68
APPENDIX A.....	69
APPENDIX B.....	xx

INTRODUCTION

Solar energy is the renewable energy source with the highest potential. The global PV sector has grown annually by an average 25% over the past two decades and by 50% over the past five years. In the future that is associated with lack of energy, PV allows access to nearly unlimited energy supply for all humankind. In an ambitious scenario PV covers 20% of global electricity consumption by 2040. Already in 2020 PV may contribute to the reduction of CO₂-emissions by an equivalent of 75 typical coal-fired power plants or 45 million cars [1]. To reach the goal that will enable the PV industry to maintain and strengthen its position on the global energy market, further developments are essential. The need for additional R/D activities is extremely pronounced if complicated binary, ternary and quaternary compound semiconductor materials are used for solar cell production.

In spite of numerous publications that have appeared in the area of compound semiconductor PV, there is yet no common approach to the processes of formation of these materials in different technological processes (electrochemical deposition, sulfurization and/or selenization of precursor metallic layers, chemical spray sputtering). Neither is there a common understanding of the influence of preparation conditions on the practically important parameters of developed materials and solar cells [2]. In these investigations, despite the huge number of different advanced methods developed to acquire in-depth insights into the materials and peculiarities of the used processes (XPS, SIMS), the traditional microscopic methods used in scanning electron microscopy (SEM) have not lost their very important position. It is justified by the development of principally new very sensitive detectors for SEM that allows obtaining very important new information and could provide new possibilities for controlling surface morphology and crystal growth, chemical and phase composition of surface and sub-surface volume of different materials in different forms [3].

Chapter 1 begins with a short account of different detection principles of SEM used in the thesis, their advantages and shortcomings. CuInSe₂ as one of the main materials used in the thesis research is described in view of its microstructure in Chapter 1, section 1. 4. A detailed literature review in field of Cu-In alloy and electrodeposited CuInSe₂ layer selenization is given in sections 1.5.-1.6.

Chapter 2 describes the methods of sample preparation and selenization, experimental microscopy and spectroscopy methods used in the thesis.

Chapter 3 presents experimental results and their discussion. The first part of this chapter reviews results in the field of selenization of co-sputtered Cu-In alloy films. The dependence of the selenization mechanism and kinetics on the selenization temperature and duration is discussed. Section 2 outlines the results in the field of selenization of sequential layers Cu-Zn-Sn films. The peculiarities of selenization of different sequence Cu-Zn-Sn layers are described. Section 3 provides the results of the investigation of the influence of thermal post-treatments in different atmospheres on the elemental composition and morphology of electrodeposited CuInSe₂ thin films.

In addition, Chapter 3 summarizes the main results obtained, presents the conclusions of the thesis and future research prospects.

ACKNOWLEDGEMENTS

This thesis is based on the experimental work carried out at the Department of Materials Science, Tallinn University of Technology.

- I would like to express my gratitude to all my colleagues for their contribution to this work.

My special thanks belongs :

- to my supervisor Professor Enn Mellikov;
- to research Professor Malle Krunk for her valuable comments and critics;
- to Dr. Julia Kois and Dr. Sergei Bereznev for help in deposition of films;
- to Dr. Jaan Raudoja for help in selenization of films;
- to MSc. Maarja Grossberg for excellent micro-Raman analysis;
- to MSc. Rainer Traksmäa and Prof Paul Barvinchi for excellent XRD investigations;
- to Dr. Daniel Abue-Ras for excellent EBSD research.

I am very grateful to the opponents – Prof. Renate Hiesgen and Prof. Dieter Meissner for their valuable time and comments.

Financial support from the Estonian Ministry of Education and Research, EU Centre of Excellence in PV Materials and Devices, Estonian Doctoral School of Materials Science and Materials Technology (MMTDK), Estonian Science Foundation (grant ETF 6179) and INTAS (Project 03-51-4561) is gratefully appreciated.

Tallinn, June 2008

Olga Volobujeva

LIST OF PUBLICATIONS

This work is based on the following original publications, which are referred to in the text by their Roman numerals:

- I. **O. Volobujeva**, M. Altosaar, J. Raudoja, E. Mellikov, M. Grossberg, L. Kaupmees, P. Barvinschi. SEM analysis and selenization of Cu–In alloy films produced by co-sputtering of metals.- Solar Energy Materials and Solar Cells, 2008, in press
- II. **O. Volobujeva**, D. Abou-Ras, M. Grossberg, J. Raudoja, E. Mellikov, R. Traksmaa. Selenization of co-sputtered Cu–In alloy films.- Proceedings of 33rd IEEE Photovoltaic Specialists Conference, San-Diego, CA, 2008, in press
- III. **O. Volobujeva**, J. Raudoja, E. Mellikov, M. Grossberg, S. Bereznev, R. Traksmaa. Cu₂ZnSnSe₄ films by selenization of Sn–Zn–Cu sequential films. was sent for publishing Journal of Physics and Chemistry of Solids
- IV. **O. Volobujeva**, J. Kois, R. Traksmaa, K. Muska, S. Bereznev, M. Grossberg, E. Mellikov. Influence of annealing conditions on the structural quality of CuInSe₂ thin films. - Thin Solid Films, 2008, 516, p. 7105-7109

In the appendix A, copies of these publications are included.

AUTHOR'S OWN CONTRIBUTION

The contribution by the author to the paper included in thesis is a followings:

- I. SEM and EDS investigations, research planning and analysis of obtained results, major part of writing.
- II. SEM and EDS investigations, research planning and analysis of obtained results, major part of writing
- III. SEM and EDS investigations, research planning and analysis of obtained results, major part of writing
- IV. SEM and EDS investigations, analysis of results, part of writing

Deposition of thin metallic films, thermal treatments of samples, XRD and RAMAN analysis were done by my co-workers.

1. LITERATURE REVIEW

1.1. Scanning electron microscopy

Solar cell devices made of compound semiconductor materials very often contain many constituents, usually in the form of stacked layers [2]. The presence of segregated phases and rough surface morphology additionally hamper the access to the quantitative information about the chemical and elemental composition of these materials and devices. In order to facilitate effective target-oriented development of materials for solar cell applications, advanced experimental methods can be used to solve structural and analytical problems inherent to the materials developed. Among those, the non-destructive microscopic methods are crucial since the compatibility for future production processes and the requirement of quality monitoring are essential for the industrial success. For example, to understand better the formation and growth of chalcopyrite compounds for solar cell applications it is essential to gain an in-depth understanding of the possible reaction paths leading to high quality materials and to identify all the crystallographic phases involved in film growth [4].

The scanning electron microscope (SEM) permits material observation and characterization on a nanometer to micrometer scale [3]. The popularity of SEM stands additionally on the capability of obtaining three-dimensional topographic images of the surfaces in a wide magnification range. In the SEM, the area of a sample is examined with a finely focused electron beam, which could be swept across the surface of the sample to form an image. The interaction of the electron beam with the sample results in signals of different types (secondary electrons, backscattered electrons, characteristic X-rays, and photons of various energies) [5]. This interaction contains different volumes within the sample (surface, sub-surface area of different thickness) that enables different microstructural characteristics of the sample (surface topography, crystal structure, composition) to be investigated. Another advantage of SEM is that it allows contrast mechanisms that are not available for other kinds of instrumentation to be used in the study and to obtain information about the crystal structure and grain orientation (EBSD). These advantages enhance the capabilities of SEM, add versatility and value to the information obtained, but at the same time make it more difficult to interpret the results.

1.2. Methods of image formation (SE, BSE, EBSD)

The interaction of focused electron beam with a specimen can be monitored in a variety of ways, allowing topographical, chemical, optical and electrical information to be obtained. This is because a variety of different phenomena occur as a result of the interaction. Some of these “phenomena” have a chance of leaving the specimen, e.g., secondary electrons and backscattered electrons, X-rays, Auger electrons and cathodoluminescence. Others tend to stay in the specimen, e.g. electrons and electron-hole pairs. Backscattering (BSE) and secondary (SE) electrons, the principal signals used to form images in scanning electron microscopy, are generated

within the interaction volume. These signals are capable of carrying information about the specimen composition, topography, local fine-scale surface texture, thickness and local inclination to the incident beam [3].

Secondary electrons are principally produced as a result of the interaction between primary electron beam and weakly bound conduction band electrons in metals or outer shell valence electrons in semiconductors and insulators. Because of low energies secondary electrons are generated near surface area, within a distance of 2-5 nm of the surface. Due to this the secondary electron detector of SEM provides the best resolution of the fine surface topographical features of the studied chalcopyrite samples. At the same time the fraction of secondary electrons produced is relatively independent of the atomic number of the scattering atoms that leads to their low compositional sensitivity [6].

Backscattered electrons are beam electrons whose trajectories have intercepted surface and which thus escape the specimen. BSE are produced as the result of elastic collisions with the atoms of the sample and usually retain about 80% of their original energy. The number of backscattered electrons produced increases with the atomic number of the specimen increasing. For this reason an investigation of the sample that is composed of two or more different elements which differ in their atomic numbers will produce an image that shows differential contrast of the elements despite a uniform topology. Elements that are of a higher atomic number will produce more backscattered electrons and will therefore be brighter than the neighbouring elements. Contrast of atomic number between the adjacent pairs of elements is strong at low atomic number and weak at high atomic number [3]. Because the backscattered electrons are usually produced by multiple scattering events, they travel considerable distances within the specimen during the backscattering process. The depth of a material from where information will be obtained using backscattered electrons detector is given by the radius of the hemispherical area, expressed as:

$$R_{BSE} \approx \frac{0.007AE_0^{1.67}}{Z^{0.9}\rho}, \mu m$$

where, A-the atomic weight, g/mole,
 Z-the atomic number,
 E-incident beam energy, keV,
 ρ-density, g/cm³.

This limits the resolution in images produced with BSE to a value that is of the order of 2R_{BSE}, regardless of how small the actual diameter of the incident electron beam may be.

Electron backscattered diffraction (EBSD) allows establishing a complete and quantitative representation of the sample microstructure. In EBSD a stationary electron beam strikes a tilted crystalline sample and the diffracted electrons form a pattern on the fluorescent screen. This pattern is characteristic of the crystal structure and orientation to the sample region from which it was generated. The diffraction

pattern can be used to measure the crystal orientation, and grain boundary disorientations, to discriminate between different materials and to provide information about local crystalline perfection. When the beam is scanned in a grid across a polycrystalline sample and the crystal orientation measured at each point, the resulting map will reveal the constituent grain morphology, orientation, and boundaries [7, 8]. Because the electrons are diffracted from very small volumes, EBSD provides high spatial resolutions. Also, simultaneous SEM micrographs and crystal orientation maps are obtained, which provide information on the crystalline properties of individual grains [8].

1.3. Analytical methods

Another type of signals produced by the interaction of the primary electron beam with the specimen is the characteristic x-rays. When an inner shell electron is displaced by collision with primary electron, an outer shell electron fall into the inner shell to re-establish the proper charge balance in its orbitals following an ionization event. The analysis of characteristic x-rays allows providing chemical information about the studied material.

EDS is well suited for chalcopyrite thin film analysis. A detailed discussion on the EDS application in chalcopyrite thin films and solar cells can be found elsewhere [9-11]. The excited characteristic X ray intensities are proportional to the total mass of the respective elements in the excited volume of a thin film absorber. The penetration ability of the electron beam depends on the used voltage of electron beam generation and that leads to various important advantages for chalcopyrite thin film analysis. Measurement results are also influenced by the morphology and homogeneity of the sample analyzed [3, 12]. Chalcopyrite thin films have a relatively rough surface and the average film thickness is varying over the whole sample area. It means that there will be slight differences in the penetration depth relative to the film thickness and the amount of the analyzed material.

The excitation of the elements is tuneable and could be changed in the range of quite large values, allowing elemental composition to be obtained either of the surface area of films or throughout the whole layer thickness. This advantage works very well in the case of homogeneous films. If there is an inhomogeneous elemental depth distribution, the measured composition will represent an average composition value. Sometimes, however, due to this, the analyzed films have to be removed from the substrate and the EDS analysis has to be done on both sides if the composition is expected to be inhomogeneous. Even if the material composition is absolutely homogeneous there could be slight changes in the output. The relative intensities of the characteristic X-ray radiation of elements when compared to one another are dependent on the excitation depth distribution. An appreciably larger error is caused if there is a depth gradient in the elemental distribution, because the output in that case is more dependent on ratio of the penetration depth to the film thickness. The error will increase if for some of the elements the L_a -lines and for others the K_a -lines are used. Besides these effects the EDS is sensitive to the angle of incidence of the electron beam, which on a rough surface can be different at various spots [3].

The distribution of the primary X-ray generation in the studied material depends mainly on the used e-beam acceleration voltage, on the material density, on the scattering of the primary electrons, on the variation of the ionization cross section with the electron energy and on some other effects. The higher the electron beam density, the higher is the excited radiation density. Therefore, the radiation generation is not homogeneous, but will be less effective in the outer region of the excited volume [3]. For thin film chalcopyrite solar cell structures and typical acceleration voltages the excited volume is of the same magnitude as the film thickness of the absorber layer. A quantitative estimation of possible errors caused by all these effects can be of the magnitude of several atomic percent.

Although all of these effects could influence the results obtained, the EDS methods could give very useful information about the composition of the material and the distribution of the elements in the volume of the materials and the methods were widely used in the thesis work.

1.4. Chalcopyrite materials for solar energy applications

As CuInSe_2 has been one of the main materials in the studies, the microstructural properties of CuInSe_2 and the methods used to modify the microstructure of these materials will be outlined below.

The ternary semiconductor CuInSe_2 is a frequently studied compound PV material [13]. CuInSe_2 belongs to the family of I-III-VI₂ semiconductor materials and crystallizes in the chalcopyrite crystal structure. This is a diamond like structure similar to sphalerite (ZnS) but with an ordered substitution of the sphalerite cations (Zn) on their sites with Cu and In . The unit cell of CuInSe_2 is shown in Fig. 1.1.

The possible phases in the system Cu-In-Se that are imported to understand the formation of the material as well as to tailor materials parameters in different post-treatments could be described on the basis of the ternary diagram Cu-In-Se (Fig. 1.2). Depending on the composition and the parameters of the used technological processes, CuInSe_2 materials with different microstructure and phase composition could be produced. The pseudobinary $\text{Cu}_2\text{Se-In}_2\text{Se}_3$ phase diagram shows that the field of the single-phase CuInSe_2 formation is wide at temperatures higher than 500°C and relatively narrow at lower temperatures.

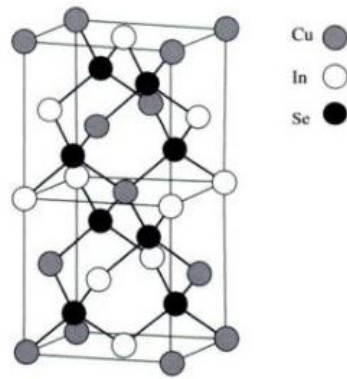


Fig. 1.1. The unit cell of CuInSe_2 [2]

The single phase region does not contain the composition 25% Cu, indicating to the In-rich composition of single phase materials at low temperatures. Considering the abovementioned, it is difficult to understand the large tolerances of CuInSe_2 parameter based solar cells on the stoichiometric composition of the used materials [2, 4]. The possible formation of ordered defect compound (ODC) phases ($\text{Cu}_2\text{In}_4\text{Se}_7$, CuIn_3Se_5 , Cu_3InSe_4) could be a possible explanation of this discrepancy [2].

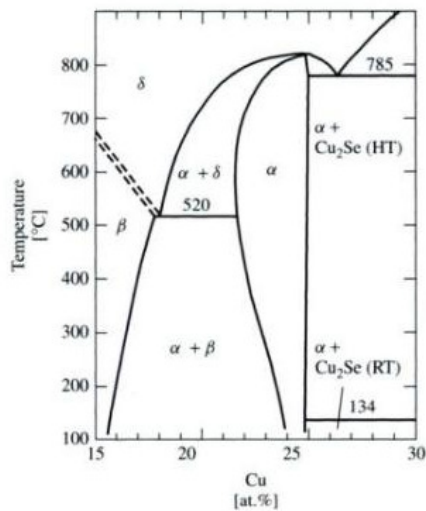


Figure 1.2. Cu_2Se - In_2Se_3 pseudobinary phase diagram [14]

1.5. Selenization of Cu-In layers

1.5.1. Introduction

Though several techniques have been reported for the growth of CuInSe_2 films, such as metal organic vapour phase epitaxy [15], molecular beam epitaxy [16, 17], flash evaporation [18], co-evaporation [19, 20], and electrodeposition [21], the

till technique technologically most favourable for the deposition of large area devices is a two-stage process in which metallic Cu-In precursor films are transferred into CuInSe_2 by means of reactive annealing [22, 23]. The strongest advantage of the two-stage processes is in the ability to use standard and well-developed techniques for metal deposition. The two-stage process of the selenization of metallic precursor layers has many variations in both the precursor metal layers deposition and in the selenization step. The precursor metal layers have been deposited by electrodeposition [24], thermal and/or electron beam evaporation [25], screen printing [26], application of nanoparticles [27] and different sequences of Cu-In alloy formation, such as bi-layers and multi-layers have been used and investigated [28, 29]. Additionally, stacked layers of Cu/In/Se or binary selenides have been used as precursors in the selenization process in various sequences and combinations [30]. A major problem of the method is the quite low homogeneity of the films after the selenization process [31]. Sputtering has a chance to solve the inhomogeneity problem and to produce metal alloy films with a smooth surface [32, 33].

The traditional two-stage process is based on the use of H_2Se as a Se source for the selenization of precursor layers. Reaction with H_2Se has the advantage of possibly precise control and use of atmospheric pressure chambers. The highest efficiency obtained for the Cu(InGa)Se_2 solar cell produced by the H_2Se selenization process is 16.2% [34]. The weak point of the H_2Se process is in the high toxicity of H_2Se that makes the technology problematic in terms of economic and ecological aspects. Thus, great efforts have been made to develop elemental Se vapour processes as alternatives [31, 35, 36]. The following literature review concentrates on the results of the investigations of composition and structure of co-sputtered and/or sequential metal precursor layers and on the peculiarities of their selenization in the vapour of elemental Se.

1.5.2. Composition of precursor Cu-In layers at room temperature

Thin films of Cu-In alloy have been the centre of interest for a long time because the chalcogenization of this alloy produces chalcopyrite semiconductors (CuInS_2 , CuInSe_2). The technique has already found industrial use for solar cell production. At the same time the dependence of the chemical nature of the phases in alloy films on their preparation has not been understood profoundly. One reason that hinders the preparation of uniform Cu-In film is the rather complex phase diagram of the Cu-In system, which consists of various intermetallic compounds. In addition, it has also been reported that in the form of thin films specific crystalline structures that do not appear on the bulk form exist in the Cu-In system [37].

Nakano [38] was one of the first to study the dependence of room temperature reactions and phase formation in vacuum deposited sequential Cu-In films on the In concentration in the precursor alloy and on the parameters of additional thermal annealing. His results indicate that the only phases in the layers between the room temperature and 75°C and at In concentrations between 50 and 75% are CuIn_2 , $\text{Cu}_{11}\text{In}_9$ and In-metal phase. Only at $[\text{In}] = 65\%$ single phase layers were produced. The results of XRD studies lead to a suggestion that this layer

consists of the intermetallic compound CuIn_2 . At indium concentrations lower than $[\text{In}] = 65\%$ the layers consist of the mixture of the phases of CuIn_2 and $\text{Cu}_{11}\text{In}_9$. Next, Nakano [36] studied sequentially deposited and heat treated Cu/In films at 120°C ($\text{In}/(\text{Cu}+\text{In}) = 55\text{--}70\%$) with XPS. The obtained results confirmed that the precursor films that were layered prior to the annealing formed into an island-like structure after the annealing. The tendency of island formation was stronger for films with higher indium content. However, no experiments were made to determine why this island-like structure forms. The roughness evolution was used as a parameter of phase formation in sequentially evaporated Cu-In films in the latest work by Nakano [39]. This approach is very interesting due to the fact that the used parameter, micro/macrosopic uniformity of the precursor films has a critical effect on the electrical and optical characteristics of chalcogenized films. The phases identified in films were Cu, In, $\text{Cu}_{11}\text{In}_9$ or CuIn_2 . The concentration of CuIn_2 increased in the samples and the concentration of $\text{Cu}_{11}\text{In}_9$ diminished toward the concentration of indium in the target $65\text{ at. } \%$. Only the CuIn_2 phase was detected in the deposited films at $[\text{In}] = 65\%$. The diffusion of copper atoms into indium was proposed as the possible mechanism of CuIn_2 formation. Upon annealing films with In/Cu ratios between 0.5 and 1 transformed and nearly single-phase $\text{Cu}_{11}\text{In}_9$ films were obtained at 150°C . The authors proposed the diffusion of indium atoms through the grain boundaries of copper as a mechanism of the formation of the $\text{Cu}_{11}\text{In}_9$ phase. Wolf et al. [40] used thin film calorimetry to investigate Cu-In alloy formation. They found that that freshly evaporated Cu–In films consist of Cu, In and CuIn_2 phases. However, when these precursors were stored at room temperature for several days in an Ar atmosphere, no indium was detected in films in favour of CuIn_2 . The authors attributed this behaviour, on analogy to the assumption of Nakano, to the rapid Cu-diffusion along grain boundaries of In that results in CuIn_2 formation [41].

The formation of a bi-layer structure with islands in the matrix area in co-sputtered Cu–In alloys was observed by Adurodija et al. [42, 43]. The number and size of the islands depend on the In concentration. Results of EDX analyses confirm that the islands are formed by elemental In and/or CuIn_2 , depending on the concentration of indium. The composition of the matrix corresponds to CuIn_2 at high In concentrations and to $\text{Cu}_{11}\text{In}_9$ at In concentrations less than 62% . They postulated that the shape and the size of the CuIn_2 islands in the matrix are determined by the difference between the surface/interface energies of the CuIn_2 phase and the underlayer. At the same time the results published by Pisarkiewicz [44] differ from those described in [39-43] and confirm in addition to $\text{Cu}_{11}\text{In}_9$ or CuIn_2 the presence of intermetallic phases of Cu_2In and CuIn in sequentially magnetron sputtered Cu/In multilayers.

R.Caballero et al. [24] deposited Cu in films in different sequences: Cu/In/Cu/In, In/Cu/In/Cu and In/Cu/In. Their results indicate that the main phase of films at room temperature for all sequences used is CuIn_{2-x} ($0 \leq x \leq 1$); additionally, the presence of metallic Cu and In in small amounts was observed. The $\text{Cu}_{11}\text{In}_9$ phase appeared only in films at the two longer sequences, Cu/In/Cu/In and In/Cu/In/Cu. W.K. Kim et al. [45] found the matrix-island structure on the surface of the as-grown Cu-In precursors. They identified the islands as an indium-rich or nearly pure indium

phase ($[\text{Cu}]/[\text{In}] = 64/36$). At the same time, the matrix was found to be Cu-rich. Results of EDS analysis by Jiang [28] confirmed that the co-sputtered metallic Cu–In alloy layers consist of indium-rich grains distributed in the matrix of the $\text{Cu}_{11}\text{In}_9$ phase.

Composition of films in more complicated In–Cu containing systems (Cu/In/Al precursor magnetron sputtered films) was studied by Zoppi [46, 47]. EDS indicates to the uniform distribution of Al, In and Cu species throughout the precursor film thickness. The XRD patterns show that the films consist of binary phases Cu_yIn_z ($\text{Cu}_{11}\text{In}_9$, CuIn_2 , $\text{Cu}_{16}\text{In}_{11}$) with various amounts of AlCu_3 and/or AlCu_4 phases as well as elemental Cu and In.

To summarize, no commonly accepted approaches exist with regard to the phase composition of Cu–In layers at temperatures near room temperatures. All the authors report the formation of intermetallic phases, but the results of different investigations refer to the different phase composition and distribution in films.

1.5.3. Influence of thermal annealing on the composition of precursor Cu–In layers

A. Ihlal et al. [48] deposited Cu–In multilayers and found that they consist of Cu and Cu–In alloy (CuIn_2), but do not contain pure In phase. Annealing at 160°C, 250°C and 400°C leads to the formation of the $\text{Cu}_{11}\text{In}_9$ phase and appearance of a peak characterizing the presence of In_2O_3 in the EDS spectra. The phase changes in the thermally annealed stacked Cu–In layers by in-situ high-energy powder diffraction were studied in detail by A. Brummer et al. [49]. They found that deposited Cu–In precursor films consist of CuIn_2 and Cu. At temperatures 75–208°C CuIn_2 reacts with free copper to form the intermetallic phase $\text{Cu}_{11}\text{In}_9$ with a release of indium melt. The $\text{Cu}_{11}\text{In}_9$ is stable up to 308°C and above this temperature it transforms into $\text{Cu}_{16}\text{In}_9$, releasing free indium. At 475–483°C $\text{Cu}_{16}\text{In}_9$ undergoes a second structural phase transition to η - $\text{Cu}_{16}\text{In}_9$ that was observed to be stable up to 550°C. Similar results were reported by Berwian et al. [50] on the basis of the investigation of stacked precursor Cu–In layers by in-situ electrical resistance measurements. They conclude that metallic stacked precursors in the layers react immediately already at room temperature, resulting in the formation of unstable CuIn_2 . Just below the melting point of In (140–155°C), the unstable CuIn_2 reacts with the remaining Cu, forming $\text{Cu}_{11}\text{In}_9$.

Very systematic in- and ex-situ study of temperature induced reactions in the system Cu–In was done by Djordjevic et al. [51, 52] using the EDXRD method. Their results follow the phase transformation sequence diagram in Fig. 1.3, where the integrated intensity of particular reflections of the observed phases is shown as a function of the process time. Besides, the Mo phase CuIn_2 and Cu phases can be observed at room temperature. Simultaneous to the vanishing of CuIn_2 reflections with the rise of temperature, the reflections refer to $\text{Cu}_{11}\text{In}_9$ and elemental indium appearance. Up to 300°C, point β , the intensity of the Cu reflections decreases, while the intensity of the $\text{Cu}_{11}\text{In}_9$ reflection increases. The intensity variations might result from the reaction of elemental Cu and elemental In to $\text{Cu}_{11}\text{In}_9$. Passing the point β , the

phase transformation $16\text{Cu}_{11}\text{In}_9 \rightarrow 11\eta\text{Cu}_{16}\text{In}_9 + 45\text{In}$ takes place. At point γ , around 320°C , only $\text{Cu}_{16}\text{In}_9$ phase was detected.

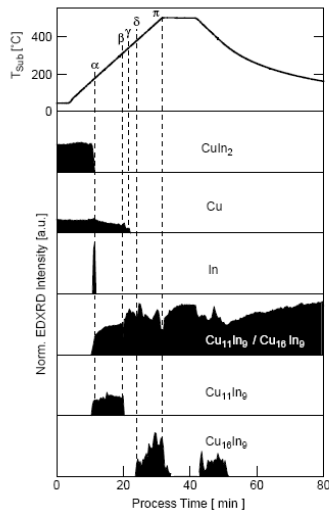


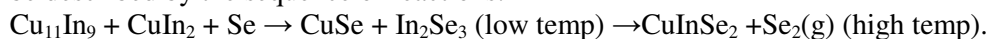
Fig. 1.3. Phase transformation sequence diagram for the annealing of $\text{Cu}_{1.8}\text{In}$ precursors up to 500°C . The substrate temperature and the integrated peak intensities are plotted versus the process time. The Greek letters indicate the phase transformations [52]

1.5.4. Ex-situ investigation of selenization of Cu-In layers in elemental Se vapour

In numerous experimental studies, the properties of the Cu-In precursor and selenized films are described in some detail [53-60]. Below a review of the results reported is given to show the necessity of additional experiments in this field. It will be shown that unfortunately, in spite of a wide range of experiments, no common approaches to the selenization process exist. Additionally, experiments do not cover in detail such important structural parameters of the precursor and selenized films as phase composition, grain size and surface topography depending on the experimental parameters of the used processes.

M. Tanda et al. [53] studied selenization Cu/In stacked layers at temperatures $340\text{-}400^\circ\text{C}$. Their results indicate that selenization at 340°C results in a multiphase composition of films (InSe , Cu_{2-x}Se , CuSe) and that the formation of single-phase CuInSe_2 films proceeds at temperatures higher than 380°C . To understand better the processes of selenization of Cu-In alloy, Rastorgi [55] studied the selenization of elemental metals, copper and indium in parallel. The obtained results indicate that the selenization of pure Cu at temperatures $340\text{-}400^\circ\text{C}$ results in the formation of CuSe and the selenization of pure In at temperatures $340\text{-}400^\circ\text{C}$ results in the formation of In_2Se_3 phase. Based on these results he proposed the mechanism of CuInSe_2 formation as the reaction between the formed binary selenides $2\text{CuSe} + \text{In}_2\text{Se}_3 = \text{CuInSe}_2 + \text{Se}$.

The selenization of co-sputtered Cu-In alloy films with different composition in elemental Se atmosphere were studied in detail by Adurođija et al. [42, 55, 56]. The authors found that the CuInSe₂ films consist of large and densely packed crystals with sizes above 5 μm and exhibit a single-phase chalcopyrite structure with preferential orientation of crystals in the (112) direction. In very In-rich compositions of precursor layers the formation of CuIn₃Se₅ defect compound was observed. The results obtained led the authors to the conclusion that the formation of CuInSe₂ could be described by the sequence of reactions:



The authors also stressed the importance of the formed CuSe phase in the recrystallization of formed films. The phase diagram of the system CuIn-2Se was constructed by Matsushita [57]. The authors indicated to several possible chemical reactions and phase transitions in the Cu+In+2Se mixture at different temperatures.

Results by J. Bekker et al. [58] show that the phase composition of selenized films depends on the Se source (H₂Se, Se vapour, Se vapour diluted in Ar) and that the efficiency of Se vapour as a selenization agent is comparable with very toxic H₂Se at temperatures over 400°C. They found that selenization in the Se vapour results in In₆Se₇, Cu₁₁In₉, CuInSe₂ and CuSe at 250°C, in In₆Se₇, CuInSe₂, CuSe and CuSe₂ at 300°C, in CuInSe₂ and CuSe at 400°C and in CuInSe₂ and CuSe_x, Cu_{2-x}Se at 500°C. Pisarkiewicz [44] selenized Cu/In multilayers in with excess elemental selenium in the temperature range 400-500°C. Selenization resulted in good quality well crystallized films with preferential orientation of CuInSe₂ in (112) plane.

The selenization of thin metallic Cu-In-Ga films of different composition and sequence was studied by Caballero [24, 59, 60]. In [59, 60] In-Ga-Cu-In sequence films were selenized in vacuum and Ar atmosphere at 500°C during 30 min. All selenized films showed a preferred orientation in the (112) plane, but the Se diffusion and the distribution of elements were critically influenced by the selenization atmosphere. An increase of grain size, a better crystallinity and a lower conductivity were observed when the selenization process was carried out in Ar containing atmosphere. In [24] different types of sequentially deposited metal layers (Cu/In/Cu/In, In/Cu/In/Cu and In/Cu/In) were selenized. After annealing at 125°C, the CuIn_{2-x} phase was mainly decomposed to Cu₁₁In₉, which was identified as the most stable state in thin films of Cu/In alloys at this temperature. After annealing at 250°C the presence of intermetallic Cu₁₁In₉, different selenized binary compounds such as Cu_{2-x}Se, CuSe₂, In₂Se₃ and InSe, as well as CIS chalcopyrite phase was detected. Despite the different reaction paths, all the sequences show single-phase CuInSe₂ with similar crystallinity and orientation of crystals in the direction of (112) in the 500°C selenized films. At the same time, the morphology of selenized films depends strongly on the sequence of layers. E.P. Zaretskaya et al. [61] studied the selenization of Cu-In co-evaporated layers in Se containing atmosphere and found that selenization at 380°C leads to single-phase CuInSe₂ films. At the same time selenization at 300°C results in multiphase films (CuInSe₂, In₂Se₃, Cu₁₁In₉, Cu_xSe). Ashour et al. [62] studied the effect of layers sequence (In/Se/Cu, In/Cu/Se, Cu/In/Se, Cu/Se/In, Se/In/Cu and Se/Cu/In) on the mechanism of the formation of CuInSe₂ thin films in reactive heat treatment. Results show that heat-treatments of different

temperature and duration are required for the selenization of precursor layers of different sequences. The best results were obtained for the sequence In/Se/Cu. In their next publication [63] the authors found a good correlation between the given peculiarities of CuInSe₂ formation and optical properties of films. Results by Ming et al. [64] indicate to the very complicated phase composition (In, Cu₁₁In₉, CuIn₂, Cu₃Ga, CuSe, Cu_{2-x}Se, InSe, GaSe) of the Cu(In,Ga)Se₂ films selenized at the temperature lower than 250°C. The rise of selenization temperature up to 560°C leads to the films where CuInSe₂, CuGaSe₂, Cu(In,Ga)Se₂ dominate.

Analogous results were reported by Jiang [28, 65]. They found the formation of chalcopyrite CuInSe₂ films after selenization for 60 min even at 230°C. However, several secondary phases such as Cu₁₁In₉, CuSe and InSe were detected. The crystallinity of films improved and secondary phases disappeared with the rise of temperature. All CuInSe₂ films exhibit preferred orientation along the (112) plane, which was enhanced by higher temperature. Based on the results obtained the authors concluded that in the early stage of the selenization process Se diffuses into metallic precursors and reacts with precursors to form selenides (CuSe and Cu_{2-x}Se, In₆Se₇ at lower and InSe at higher temperatures) and proposed that the formation of CuInSe₂ proceeds by a reaction $\text{CuSe}(\text{Cu}_{2-x}\text{Se}) + \text{InSe}(\text{In}_6\text{Se}_7) \rightarrow \text{CuInSe}_2$. Higher selenization temperatures accelerate the Se incorporation and reduce the time of formation of CuInSe₂ phase.

One of the widely discussed aspects of the selenization of metallic layers is the possible loss of Se and In during the high temperature selenization. This aspect is of particular concern in the technology of CuInS₂ solar cells and has resulted in the use of rapid thermal annealing. V. Alberts, M.L. Chenene [66] studied the selenization of selenium-free (Cu/In/Cu, In/Cu/ In) and selenium containing (InSe/Cu, Cu/InSe) films in H₂Se containing atmosphere at 450C. No component loss was found in the selenization process. At the same time Klenk [67] observed a remarkable loss of In and Se in the thermal treatment due to the formation of volatile In₂Se and Ga₂Se phases during growth, resulting in a copper-rich surface layer. Their results confirm that the continuous supply of selenium (the maintenance of Se overpressure) is of greater importance during CuInSe₂ growth than for CuGaSe₂ growth.

To summarize, we can conclude that the results obtained are contradictory and no common view has been accepted of how the composition and structure of selenized layer is influenced by the parameters of selenization and the composition of precursor layers. Ex-situ investigations of selenization have not led to a common understanding of the mechanism of formation CuInSe₂ and the obtained results are often overshadowed by the processes during the cooling of samples. Due to this during the last few years several in-situ investigations of selenization have proceeded and results have been published.

1.5.5 In-situ investigation of selenization process of metal layers in elemental Se vapour

Two-step preparation of chalcopyrite thin-films is governed to a large extent by phase formation kinetics, which has to be known in detail to optimize the process.

The knowledge of the phases involved in the chalcopyrite formation in process conditions is essential for the development of an understanding of the growth process. Ex-situ studies have given only very limited information about the phase formation and the information obtained is often twisted due to processes during cooling. During the last few years intensive in-situ investigations of chalcogenization of precursor layers with different nature and composition have been conducted to get more precise insight to the process [40, 45].

Wolf [40] investigated CuInSe_2 formation from Cu-In-Se stacks by thin film calorimetry during thermal annealing at temperatures up to 550°C . The results obtained indicate that up to roughly 310°C , $\text{Cu}_{11}\text{In}_9$ and $\text{In}(\text{Cu})$ react with Se to form binary selenides. The formation of In-selenides is controlled both by temperature and by the phase composition of the Cu-In alloys. The reaction of Cu and Se proceeds in two steps: rapid diffusion of Cu is responsible for the formation of CuSe , which is subsequently followed by the formation of CuSe_2 at a significantly lower rate. CuInSe_2 formation at higher temperatures is governed by slow inter-diffusion of binary phases. A. Brummer et al. [49] studied the formation of CuInSe_2 by the annealing of stacked Cu/In/Se layers using in-situ high-energy powder diffraction. Their results indicate that the initial stage of the precursor transformation is governed by the formation of $\text{Cu}_{11}\text{In}_9$ from Cu and CuIn_2 and by the subsequent decomposition of $\text{Cu}_{11}\text{In}_9$ and above 308°C $\text{Cu}_{16}\text{In}_9$. The melting of Se between 208°C and 225°C triggers the decomposition of the $\text{Cu}_{11}\text{In}_9$ due to a sluggish reaction of $\text{Cu}_{11}\text{In}_9$ with the molten Se. The compound CuSe_2 forms together with CuSe , In_4Se_3 and at 275°C with Cu_{2-x}Se . At all temperatures poor in selenium indium selenides form in spite of the fact that it occurs in the presence of molten selenium in excess. The affinity of Se to form the copper selenides seems to be higher and consumes the larger fraction of the Se. Only once the $\text{Cu}_{16}\text{In}_9$ decomposition is finished, the three phases In_4Se_3 , CuSe and CuSe_2 become unstable and transform into InSe and Cu_{2-x}Se . CuInSe_2 finally forms from these two phases and the Se rich melt starts at a temperature of $375\text{--}383^\circ\text{C}$.

Results by W.K. Kim et al. [45] indicate that during the selenization of Cu-In by temperature ramp annealing ($20^\circ\text{C}/\text{min}$) the formation of CuSe and its transformation to CuSe_2 , following the transformation of CuSe_2 to CuInSe_2 occurs in the temperature area from 230°C to 300°C . The onset of the formation of CuInSe_2 was observed at a temperature between 250°C and 300°C . The formation of MoSe_2 was detected only at temperatures above 440°C after the formation of CuInSe_2 was complete. In the case of insufficient amount of Se in the system it results in the formation of CuInSe_2 without producing MoSe_2 even after 440°C . Analogous studies with similar results were performed by the same group for Ga containing systems [68, 69].

Hergert et al. studied the formation of CuInSe_2 (CuGaSe_2) of different precursors in Se atmosphere: metallic precursor layers [70], stacked binary layers [71], in differently deposited and composed stacked elemental layers [72], and electrochemical precursors [73]. The used stacked metallic precursors consist of $\text{Cu}_{11}\text{In}_9$ and CuIn_2 [70].

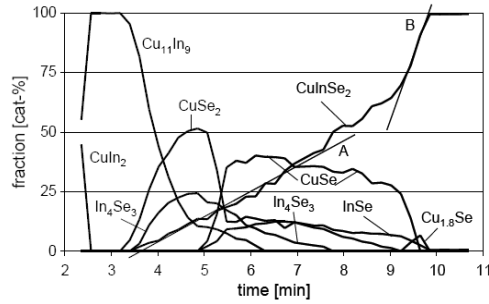
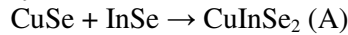
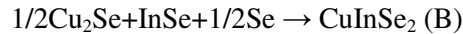


Fig. 1.4. Time dependent phase content in Cu/In/Se precursor. Note the two-stage process forming CuInSe_2 via reactions (A) and (B) [70]

The formation of binary selenides in selenization coincides with the melting of Se (Fig. 1.4). The binary CuSe_2 forms the beginning of rapid thermal annealing due to Se excess. In the following reaction path CuSe_2 serves as a buffer for Se. Its partial decomposition delivers Se for the selenization of In_4Se_3 to In Se by the reaction: $\text{CuSe}_2 + \text{In}_4\text{Se}_3 \rightarrow \text{CuSe} + 4\text{InSe}$ well below its thermal decomposition temperature. At higher temperatures contents of CuSe_2 and CuSe decrease. As the fraction of CuSe_2 still increases during the growth of CuInSe_2 authors conclude that CuInSe_2 is not formed by reaction of CuSe_2 with InSe, but via the reaction:



At 650K CuSe decomposes into Cu_2Se and Se. Once CuSe decomposes at 650K a rapid increase in the formation rate of CuInSe_2 is observed, indicating a change of the reaction mechanism



Thus, a two-stage process of CuInSe_2 crystallization is observed. The first reaction that involves CuSe starts at the Se melting point and is slow. The second starts abruptly at the decomposition of CuSe into Cu_2Se and is faster. The same authors report [72] that the processes of CuInSe_2 formation are similar in differently deposited and composed stacked elemental layers. Small differences were determined only in the temperature scale of different reactions, but the mediate phases of CuInSe_2 formation were principally the same.

Very systematic in- and ex-situ study of the selenization and temperature induced reactions in the system of Cu-In layers was done by Djordjevic et al. [52,77] using the EDXRD method. The investigated samples were poor in Cu composition. Selenization results of $\text{Cu}_{0.8}\text{In}$ precursor layers in the ramp reactive heated up to 550°C could be described as shown in Fig. 1.5. The crystalline phases observed with EDXRD are CuIn_2 and Cu (spectrum (A) at 44°C); $\text{Cu}_{11}\text{In}_9$, In_4Se_3 , InSe and CuInSe_2 (spectrum (B) (325°C)) and $\text{Cu}_{16}\text{In}_9$ and CuInSe_2 (spectrum (C) (534°C)). The investigated films reveal that the phase transformation $\text{CuIn}_2/\text{Cu}_{11}\text{In}_9$ occurs at around 150°C . This transformation proceeds via release of liquid In until after this transformation peaks referred to elemental In appear. At around 300°C , the second intermetallic phase transformation $\text{Cu}_{11}\text{In}_9/\eta\text{-Cu}_{16}\text{In}_9$ takes place under the release of liquid In.

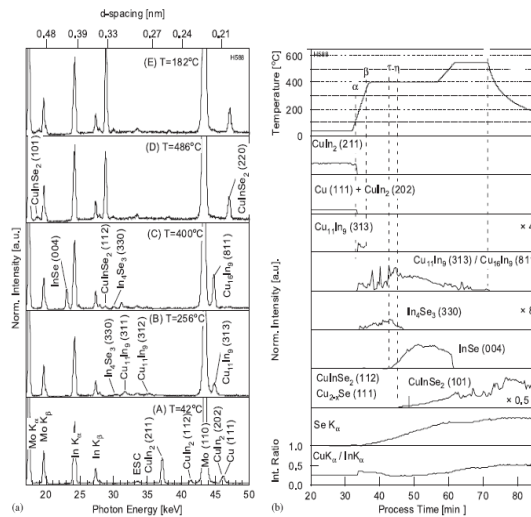


Fig. 1.5. Selenization of a $\text{Cu}_{0.8}\text{In}$ precursor layer. (a) Energy dispersive X-ray diffraction spectra are recorded at $T_{\text{sub}} = 40^\circ\text{C}$ (A), at $T_{\text{sub}} = 260^\circ\text{C}$ (B), at $T_{\text{sub}} = 400^\circ\text{C}$ (C), at $T_{\text{sub}} = 490^\circ\text{C}$ (D), and in the cool-down period at $T_{\text{sub}} = 180^\circ\text{C}$ (E). All spectra are normalized to the MoK_α fluorescence line. (b) Temperature profile and determined intensities of selected reflections as a function of the process time [79]

To summarize the results of in-situ investigations, we can conclude that In- and Cu-binary phases play an important role for the growth of CuInSe_2 and chalcopyrite growth is reaction limited. No remarkable differences exist in phase formation in the ternary system Cu-In-Se and in the separate binary systems Cu-Se and In-Se. The only difference is that due to greater affinity of Se to Cu, reactions of Cu with Se prevail reactions between In and Se, leading to the changes in the onset temperature and the level of some reactions between In and Se.

1.5.6. Sulphurization of metallic films

XRD spectra of the layers sulphurized at 160 to 400°C indicate the existence sphalerite CuInS_2 phase at all layers sulphurized at different temperatures [48]. The preferential orientation of the formed CuInS_2 was in the (112) plane. In [80] $\text{Cu}_{11}\text{In}_9$ films were reactively annealed in sulphur vapour. The results indicate to an indium loss of close to 50% during sulphurization at 500°C due to the volatilization of the In_2S compound formed at mediate temperatures. A large sulphur excess was necessary in order to obtain stoichiometric CuInS_2 during long sulphurization times. As the formation of In_2S is favoured by the phase transition of $\text{Cu}_{11}\text{In}_9$ to $\text{Cu}_{16}\text{In}_9$ at 307°C , they proposed sulphurization at the temperature of 300°C as optimal for CuInS_2 film production. I. M. Kötschau et al. [82] found significant changes with the level of sulphur pressure in the reaction pathway and in the secondary Cu-S phases which segregate on top of the CuInS_2 films. The formation of binary In-S and Cu-S phases and the ternary CuIn_5S_8 phase were found before the formation of the

chalcopyrite phase. Ch. von Klopmann et al. [78] found several differences in the CuInS₂ formation as compared to CuInSe₂ formation. Their results show that CuInS₂ growth takes place via decomposition of Cu₁₆In₉ and is diffusion-limited.

The metal targets of Cu, Zn and Sn were sulfurized at the temperature region of 250°C to 580°C [83]. The precursor Cu-Zn-Sn alloy consists of Cu₃Zn₈ and Sn, the formation of CuSn was observed at 250°C. Consequently, Cu₆Sn₅, CuSn and ZnS were formed at 350°C. The films sulphurized at 450°C consist basically of kesterite-phase CZTS and of extremely few SnS in. Annealing at 580°C results in the single-phase CZTS. Raman spectra of sulphurized films reveal peaks responsible for ZnS phase at all sulphurization temperatures (250-580°C). The peaks corresponding to the sulphides of Cu and Sn were not observed. The uniform distribution of Cu was observed both in the precursor and in the films sulfurized at high temperature.

The formation of Cu₂ZnSnS₄ thin films by annealing of stacking: Mo/CuS/ZnS-SnS) films in sulphur atmosphere were investigated by in-situ energy dispersive X-ray diffraction [84]. The films were annealed at temperatures up to 550°C. ZnS, CuS, Cu_{2-x}S, Sn₂S₃ and SnS were found as main binary phases during annealing. It was shown that the Sn₂S₃-SnS phase transition has a significant impact on the formation of ternary/quaternary phases. The rapid crystallization of Sn₂S₃ takes place at 200°C. Further heating leads to abrupt phase transition from the Sn₂S₃ to the not stable SnS phase that decomposes gradually. The little influence of the precursor stacking on the reaction path was explained with the high diffusivity of copper. The coexistence of ternary copper tin sulphides Cu₂ZnSnS₃ and quaternary Cu₂ZnSnS₄ in high temperature films was proposed.

1.6. Thermal annealing and selenization of electrochemically deposited films

The electrodeposition of CuInSe₂ differs from the classical vacuum based processes mainly by the way the absorber is prepared. At the same time this difference leads to several differences in phase composition, stoichiometry and electrophysical parameters of active layers of solar cells [21]. All of this makes the preparation of active layers for solar cells in the use of electrodeposition questionable.

During the last years Jost et al. have shown on the basis of real-time formation investigations [73, 85-87] that electrochemical deposition could lead to three different types of precursor films that have different phase composition and surface morphology. The observed differences exert a strong influence on the CuInSe₂ formation mechanism in the post-annealing process as well as on the resulting absorber morphology and composition [85]. The overall characterization of these initial films is given in Table 1.1 [73]. Precursor film type I comprises the nanocrystalline as-deposited phases Cu_{2-x}Se and InSe, which react to the chalcopyrite CuInSe₂ starting at an annealing temperature of 470K. Precursor film type II shows an inhibited CuInSe₂ formation from the initial precursor γ -In₂Se₃ and Cu_{2-x}Se starting already at 400K. The chalcopyrite crystallization of type III electrodeposited

precursor films is completely different. The intermetallic phase $\text{Cu}_{11}\text{In}_9$ that is present in precursor films reacts with elemental selenium to binary copper and indium selenides at sample temperatures around the melting point of selenium at 494K. After selenium transfer reactions the chalcopyrite CuInSe_2 is formed from the phases Cu_{2-x}Se and InSe starting at a temperature of around 670K. This chalcopyrite formation mechanism is similar to the chalcopyrite formation mechanism for the vacuum produced precursor films produced by sputtering and thermal evaporation of the elements [52, 70, 74]. In contrast to type I and II precursor films, the absorber surface for III precursor films consists of CuInSe_2 crystallites with a grain size in the micrometer range.

The authors show that the amount of selenium deposited during the simultaneous electrodeposition of copper, indium and selenium is the key parameter to determine the parameters of precursor films and the possibility to achieve semiconductor formation similar to vacuum deposited films. The simultaneous electrochemical deposition of copper, indium and selenium in the ratio near stoichiometric CIS leads to the formation of binary copper and indium selenides during the deposition process. These binary selenides serve as direct educts for the formation of the chalcopyrite CuInSe_2 in the annealing process (films described as type I and type II precursors). A reduced amount of electrodeposited selenium leads to the existence of the intermetallic precursor phase $\text{Cu}_{11}\text{In}_9$, which is decisive for vacuum deposited films similar to CIS formation. In this case, the missing amount of selenium must be deposited in a second electrochemical bath or by the additional thermal annealing process (resulting in the composition of the chalcopyrite with $[\text{Se}] / ([\text{Cu}] + [\text{In}]) = 1$).

Table 1.1. CuInSe_2 formation mechanisms of different electrodeposited precursor types

	type (I)	type (II)	type(III)
initial precursor phases	Cu_{2-x}Se and InSe	Cu_{2-x}Se and $\gamma\text{-In}_2\text{Se}_3$	$\text{Cu}_{11}\text{In}_9$ and Se
chalcopyrite formation	from initial phases	from initial phases	formation of binary selenides above the melting point of Se , CuInSe_2 formation from Cu_{2-x}Se and InSe
Temperature of chalcopyrite formation	470 K	400 K	670 K

At the same time none of the as-electrodeposited precursor films are in electronic quality and need thermal annealing post-treatments to obtain high quality films. In spite of that the above considerations make a strong difference between the

differently electrodeposited films and determine that only III type of precursor films need thermal annealing in Se, several studies were conducted in different research laboratories for the optimization of the precursor properties (composition, structure) of films using different thermal annealing step parameters (temperature, duration) and different Se non-containing [88-95] and containing [48, 96-102] atmospheres.

1.6.1. Annealing electrodeposited films in Se non-containing atmospheres

Authors of works annealed one-step deposited films under neutral atmosphere in vacuum at temperatures 400-550⁰C [88, 89]. Their results show that thermal treatment leads to the improvement of the structural and optical properties but not to remarkable changes in the electronic properties of films. Electrodeposited CIS precursor films were annealed in high vacuum for a short time at the temperature of 550⁰C in [90]. Annealing leads to more compact relatively small-crystalline single-phase films with improved crystal structure and CIS, In₂Se₃ and Cu₂Se in.

Results of investigations by XRD, SEM and EDS in [91] indicate also to the improvement of crystalline structure of one-step electrodeposited amorphous Se rich CIS and CIGS precursor films after annealing in vacuum at 450⁰C. Similarly to [90] they found that the Se content in CIS films decreased slightly after annealing, but at the same time films stayed Se-rich. In [92] one-step electrodeposited CIS thin films were annealed in nitrogen at different temperatures. The authors found that only annealing of films at higher temperatures, at 400⁰C, leads to the formation of CIS and to the improved crystallinity of films. At the same time a remarkable amount of binary compounds, such as CuO, Cu_xSe, was detected. In their study the authors of [93] annealed as-deposited CuGa/CIS bilayers in argon atmosphere to modify their structure, composition and properties. The obtained results suggest that annealing at 600⁰C for 60 min allows preparing uniform CIGS films with the composition determined by thicknesses of CuGa and CIS layers. In [94] authors annealed one-step electrodeposited CIS and CIGS films under vacuum at different temperatures. The annealing in vacuum at low temperatures, at 200⁰C, increases grain size in the films but in addition to CuInSe₂ leads to intermediate phases, such as Cu₂Se and In₂Se₃ in films. These phases disappear at the annealing temperature of 400⁰C, as they react together to form CuInSe₂ and single-phase CIS films with well formed crystalline structure were obtained. The authors found a loss of selenium from films during the annealing. Calixto et al. [95] studied in detail the process of CIS film formation in the electrodeposition process. They concluded that the electrodeposition leads always to higher concentration of Cu in the bottom layer and to the higher concentration of In in the upper layer of films. As-deposited films were in a semi-crystalline structure with very small grains in. Films annealed at 500⁰C are polycrystalline with grain sizes larger than 1 μm but without any preferred orientation of grains.

1.6.2. Annealing of electrodeposited films in the Se containing atmosphere

The influence of annealing treatments of one-step electrodeposited films in a selenium atmosphere was investigated in [96]. The substrate temperature was 450⁰C

and selenium pressure was varied from 0 to 10^{-1} atm (unlimited Se source). As-grown films were poorly crystallized, with grain sizes of few tens of nanometres. The annealing at the selenium pressure ($p_{\text{Se}} \geq 10^{-3}$ atm, $T_{\text{Se}} \geq 350^{\circ}\text{C}$) improves the crystal structure of films and results in films with preferential orientation along the $\langle 112 \rangle$ direction. Large monocrystalline grains which extend over the whole thickness of the layer appear in annealed films.

A. Ihlal et al. [48] studied in parallel the selenization of sputtered and electrodeposited films. Annealing of films in the selenium atmosphere led to the formation of the chalcopyrite CuInSe_2 with the preferential orientation in the (112) plane and with crystals size larger than 40 nm. Both the morphology and crystal structure of selenized films depend on the parameters of electrodeposition. 400°C was determined as the optimal temperature for selenization, leading to the compact morphology of films and to the homogeneous composition of grains. Sene et al. [97] electrodeposited CuInSe_2 thin films on Mo/glass substrates by one-step electrodeposition from aqueous baths. Selenization in H_2Se improves crystalline properties and helps to identify the chalcopyrite crystal structure of the films. One step electrodeposited CuInSe_2 thin films were annealed in an atmosphere of selenium at 500°C and analyzed using XRD, SEM by [98]. The electrodeposited precursor films were in the tetragonal chalcopyrite structure without any binary phases (Cu_2Se). The authors noticed a fibre-like growth attributed to an In-rich phase on the surface of the electrodeposited CIS films that disappeared after annealing in Se.

Shivagan et al. [99] characterized by XRD, SEM, EDS, photocurrent spectroscopy and EER electrodeposited Cu-In precursor films before and after selenization in elemental Se atmosphere at 500°C . The annealing of as-deposited almost amorphous Cu-In films at 170°C leads to the formation of $\text{Cu}_{11}\text{In}_9$ and elemental In in films. The selenization at 500°C for 30 min was needed to convert Cu-In precursor films fully to the single-phase CIS. In the next paper [100] single-bath electrodeposition of CuInSe_2 and $\text{Cu}(\text{In,Ga})\text{Se}_2$ was carried out from buffered low concentration baths. The resultant CuInSe_2 and $\text{Cu}(\text{In,Ga})\text{Se}_2$ films are smooth, compact, but low crystalline. The authors found that the composition of electrodeposited CIS film does not change considerably after selenization, though some loss of Se exists. The analysis of XRD patterns indicates to the significant recrystallization and to the formation of MoSe_2 at a temperature higher than 450°C . It was shown that recrystallization begins within the first few minutes of annealing and is generally completed during 20 minutes.

The influence of selenization on the structure and composition of films electrodeposited with a variety of electrochemical bath compositions and in use of different growth procedures was studied in [101]. Two types of annealing procedures were employed to obtain homogeneous CIS films: annealing in air at 500°C and annealing in selenium atmosphere at 500°C . Annealing in air improves the quality of the films and the films become more compact, uniform as well as stoichiometric. Annealing in an optimized Se pressure (10^{-2} atm) yields in stoichiometric, uniform and nanostructured CIS deposits. Electrodeposited sequential Cu- In layers at different Cu to In ratios were annealed at 550°C in a chamber containing saturated H_2S gas alloy in [102]. It was found that single-phase polycrystalline CuInS_2 with a chalcopyrite

structure and good morphology can be obtained by optimizing the thickness of the initial Cu and In layers.

1.7. Summary and goals of the research

The knowledge of the phases involved in the chalcopyrite formation at process conditions is essential for the development of an understanding of the growth process. One reason that hinders the preparation of uniform Cu–In film is the rather complex phase diagram of the Cu–In system, which consists of various intermetallic compounds. The dependence of the chemical nature of phases in alloy films on their preparation has not been understood till profoundly and several phases appear only in the thin film form. Selenization of Cu-In thin-films is governed to a large extent by phase formation kinetics, which has to be known in detail to optimize the process. Due to this the results of selenization are contradictory and there is no common view how the composition and structure of the selenized layer is influenced by the parameters of selenization and the composition of precursor layers. Ex-situ studies have given only very limited information about the phase formation and information obtained is often twisted due to processes during cooling. In-situ investigations allow us to get a more precise insight to the process and to conclude that the sequence of phase transformations during the annealing of Cu-In films could be successfully explained by the phase diagram.

There are no publications describing phase composition of differently sequenced Cu-Zn-Sn layers and the formation of $\text{Cu}_2\text{ZnSnSe}_4$ in the process of their selenization. At the same time $\text{Cu}_2\text{ZnSnSe}_4$ is one of the most perspective materials for thin film solar cell adsorber materials and several laboratories and companies had opened development activities with this material.

The as-electrodeposited precursor films are not in electronic quality and they need thermal annealing post-treatments to obtain high quality films. Several studies were conducted in different research laboratories for the optimization of the electrical parameters of precursor films using different thermal annealing step parameters (temperature, duration) and different Se non-containing and containing atmospheres, but insufficient attention has been given to the changes in the structure and composition of electrodeposited films in post-treatment processes.

Following above-given the aims of the research by the dissertation are as follows:

- a. Investigation of the mechanism of selenization of different metallic alloy and stacked precursor layers
- b. Development of thin CuInSe_2 and $\text{Cu}_2\text{ZnSnSe}_4$ films with tailored morphology, phase composition and structure
- c. Investigation of the influence of different thermal and chemical post-treatments of morphology, composition and structure electrochemically deposited precursor films.

2. EXPERIMENTAL

2.1. Deposition of precursor metallic films

2.1.1 Deposition of precursor copper–indium alloy films

The precursor copper–indium alloy films were formed on molybdenum covered soda-lime glass substrates by magnetron sputtering of Cu/In alloy targets in Scheuten Glasgroap. Alloy films were sputtered on the glass substrates at ambient temperature. High purity (99.998%) argon plasma was used during the co-sputtering process. The applied power density of 0.8 watt/cm² leads to a deposition rate of approximately 1 nm/sec. The total thickness of the Cu/In alloy films of 1000 nm was adjusted by the layer sputtering time. The ratio of Cu to In concentrations of films ([Cu]/[In]) was controlled by the composition of Cu-In alloy target ([Cu]/[In] = 0.88).

2.1.2. Deposition of precursor copper–zinc-tin sequential films

The precursor films (Sn-Zn-Cu) with different sequence were deposited onto molybdenum (Fig. 2.1) covered soda-lime glass substrates by vacuum evaporation. Different parameters of deposition (sequence of layers substrate temperature, substrate temperature, temperature of vacuum post-treatment) were used to determine optimal deposition parameters for the CZTS films formation following. The thickness of the precursor films was adjusted by the use of oscillatory quartz crystal microbalance and was controlled by the evaporation time and/or by SEM measurements. Differences in deposition parameters result in the precursor films with different composition and thickness (Table 2.1.).

Table 2.1. Deposition process parameters of precursor CZT films

No	Sequence of layers	Substrate temperature, °C	Temperature of vacuum postannealing, °C	Thickness of film, µm	Composition of precursor Cu:Zn:Sn
1	Sn-Cu-Zn	550	no	550	(Cu/Zn)=1.8 Zn/Sn=1.2 Cu/(Zn+Sn)=1.0
2	Zn-Cu-Sn- Zn-Cu-Sn	120	200	550	(Cu/Zn)=1.4 Zn/Sn=1.8 Cu/(Zn+Sn)=1.9
3	Cu-Zn-Sn	150	no	550	(Cu/Zn)=2.7 Zn/Sn=0.9 Cu/(Zn+Sn)=1.3
4	2Cu/Sn-Zn	150	no	800	(Cu/Zn)=1.9 Zn/Sn=0.95 Cu/(Zn+Sn)=0.9
5	2Cu/Sn-Zn- 2Cu/Sn-Zn	150	no	550	(Cu/Zn)=1.9 Zn/Sn=0.9 Cu/(Zn+Sn)=0.95

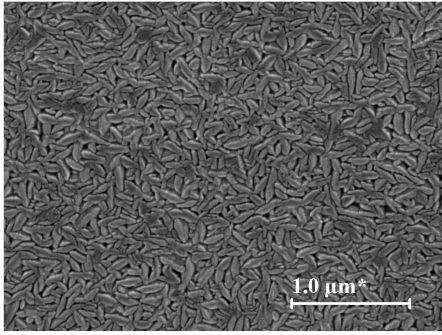


Fig. 2.1. Surface of Mo covered glass substrate for CuInSe_2 deposition

2.1.3. Electrodeposition of CIS films

Aqueous solutions of CuSO_4 , $\text{In}_2(\text{SO}_4)_3$ and SeO_2 were used as component sources for CuInSe_2 film electrodeposition onto Mo covered substrates. Aqueous solutions of CuCl , InCl_3 and $\text{Ga}(\text{NO}_3)_3 \cdot 7\text{H}_2\text{O}$ were used as component sources for Cu-In-Ga films deposition. The electrochemical deposition process is described in detail in [103]

2.2 Selenization of metallic and electrochemically deposited CIS films

Elemental Se was used for the selenization of Cu–In alloy, Cu-Sn-Zn stacked layers and electrochemically deposited CIS films. Two different experimental setups were developed and used for the selenization process: a) selenization in an isothermal sealed quartz ampoules, in which the Se pressure was controlled by the amount of elemental Se in the ampoule and by the temperature of the selenization process; b) selenization in two temperature zone sealed quartz ampoules, in which the Se pressure for the selenization process was determined by the temperature of the lower temperature zone of the ampoule. The temperature of selenization was varied from 210 to 550°C; the duration of the selenization was between 0.25 and 2 hours. Se pressure was varied between 0.01 and 25 Torr. At the end of annealing, samples were pulled out and cooled down to the room temperature.

The electrochemically deposited films were thermally annealed in an elemental selenium atmosphere to form the CIS. A horizontal furnace was used for the annealing of the electrodeposited films in dynamic vacuum. The annealing process is described in detail in [IV].

2.3 Methods of sample characterization

Evolution of the surface morphology and the crystalline structure of the studied thin films were analyzed by the high resolution scanning electron microscope (HR SEM) Zeiss ULTRA 55 equipped with the In-Lens SE detector for topographic

imaging and energy and an angle selective backscattered detector (EsB) for compositional contrast. The samples were investigated mainly in low voltage modes that allow to avoid charging of surface during SEM observations and to investigate uncoated samples. The used excitation voltage was in the range of 1.5 -2 keV and a current aperture of 30 μm .

The SEM specimen for surface morphology studies were prepared by gluing the investigated film with conductive glue onto the conductive substrate. For cross-section sample preparation the investigated films were broken and it was assumed that the samples break along the grain boundaries of the polycrystalline layers. After that samples were analogously glued to the surface with opened cross-sectional part top. After drying of glue the specimen were carefully cleaned in plasma cleaning chamber from the possible organic contamination of investigated surface that could influence the results of morphology investigations. Additional mechanical polishing before measurements was used only for very rough surface samples.

The electron backscattered diffraction (EBSD) (or backscatter Kikuchi diffraction) patterns were used for the microstructural characterisation of developed films. In difference of other methods of determination of orientation of crystals in films the EBSD allows to deal with small group of contiguous microscopic crystals. In our study EBSD was applied only to the measurement of texture, i.e., the mapping of the orientation of individual grains in selenized at high temperature films. The EBSD measurements were performed in the SEM laboratory of Hahn Meitner Institute (HMI, Germany) in use of a LEO GEMINI 1530 SEM equipped with an Oxford Instruments HKL NordlysII-S EBSD detector. The applied in investigations excitation voltage was 20 kV and the probe current was about 1 nA. The EBSD patterns were acquired and evaluated using the Oxford Instruments HKL software package CHANNEL5. EBSD linescans and maps were recorded with point-to-point distances of 10-50 nm and with recording durations ranging from 120 ms to 1 s at each point. Crystallographic contrast of EBSD permits to image grains with different orientation in different colours in EBSD maps. As the electrons are diffracted from very small volumes, the EBSD provides high spatial resolutions, unlike other techniques, such as X-ray diffraction. The simultaneous SEM micrographs and crystal orientation maps were recorded, which allows to provide information on the crystalline properties of individual grains and to reveal twin crystals and grain boundaries in films.

For EBSD measurements, samples studied were prepared by cutting slices from thin film solar cells, forming stacks by face-to-face gluing of two slices, and by careful polishing of the cross-sections, followed by ion-polishing. Deposition of very thin (about 4-5 nm) graphite layers on the cross-sections reduced the sample drift during the acquisitions. The kind help of Dr. D. Abue-Ras in sample preparation and in EBSD measurements was very valuable.

The chemical composition and stoichiometry of prepared thin film precursor and chalcopyrite materials and the distribution of components in investigated films were determined using an energy dispersive x-ray analysis (EDX) system (Röntec XFlash 3001 detector). Additionally EDS was used to determine lateral uniformity and in depth compositional uniformity of developed films. The advantages of EDS

are that this method is destruction free and allows quick analysis with very high lateral resolution. The main problem with the EDS as a tool for analyze was that the samples with smooth surfaces were needed for high precise analyze. Due to this strong attention was given to the preparation of samples for EDS analyze. The EDS specimen for surface composition analyze were prepared by gluing the investigated film with conductive glue onto the conductive substrate. For cross-section sample, the investigated films were broken and it was assumed that the samples break along the grain boundaries of the polycrystalline layers. After that samples were analogously glued to the surface with opened cross-sectional part top. After drying of glue the specimen were carefully cleaned in plasma cleaning chamber from the possible organic contamination of investigated surface. Additional mechanical polishing before measurements was used only for very rough surface samples

Another problem with the use of EDS analyzes in investigation of our thin alloy and stacked films with complicated element distribution was fundamentally connected with the process of excitation of characteristic radiation by an impacting SEM electron beam. The generation and distribution of the characteristic X-ray radiation depends mainly on the e-beam acceleration voltage, the material density and the variation of the ionization cross section of different film composite elements with the excitation energy. The excited depth (volume) depends strongly on e-beam acceleration voltage. The higher electron density in upper volume of investigated sample leads to the higher excited radiation density in this area. Therefore, the characteristic radiation generation is not always homogeneous, and is less effective in the lower (outer) part of the excited volume. It leads to the slight fluctuations in results if the investigated samples are not homogeneous (in volume or in depth). To avoid the influence of unhomogeneity to the results of EDS analyze, the films were investigated always using different e-beam acceleration voltages keeping in mind the calculated penetration depths of used e-beam and excitation energies of investigated elements. It was especially important in investigation of total amounts of constituent elements in sequential samples where an appreciably larger error (the magnitude of several atomic percent) was noticed in results of analyze if incorrect e-beam acceleration voltage was used. Due to this in the case of determination total amounts of constituent elements in sequential samples the e-beam acceleration voltage was used that leads to the appearance of small lines of elements from the substrate. Typical values of e-beam acceleration voltage used for EDS were in range of 7-20 keV.

Bulk structure and phase compositions were additionally studied using X-ray diffraction (XRD) and Raman spectroscopy. A Bruker D8 ADVANCE diffractometer was used to identify the phases of the films. Cu K_{α} was used as an X ray source (40 kV, 40 mA) in the Bragg-Brentano geometry. XRD investigations were done by Prof. P Barwinski from University of Timisoara, Romania and by R.Traksmaa, Tallinn University of Technology. The XRD peaks were identified using JCPDS fails [104].

The room temperature (RT) micro-Raman spectra were recorded by using a Horiba's LabRam HR high resolution spectrometer. The incident laser light with the wavelength of 532 nm was focused on samples within a spot of 1 μm in diameter and

the spectral resolution of the spectrometer was about 0.5 cm^{-1} . Raman measurements were performed at our laboratory by Maarja Grossberg.

3. RESULTS AND DISCUSSION

3. 1. Selenization of Cu–In alloy films produced by co-sputtering of metals

The results of research in this field have been published and are described in (I and II in Appendix A).

3.1.1. Precursor copper and indium alloy layers

The copper–indium alloy films were deposited on molybdenum covered soda-lime glass substrates at ambient temperature by magnetron sputtering of Cu/In alloy targets. Sputtered Cu–In alloy films exhibit a rough bi-layer structure of the surface in which island - type crystals were formed in a “small-crystalline” matrix layer (Fig. 3.1.). The cross-sectional SEM image of an In-Cu alloy film (Fig. 3.1a) indicates that island - type crystals extend through the matrix layer down to the Mo layer. Results of the EDS analysis show that the matrix area of co-sputtered Cu–In alloy layers is Cu-rich (Cu/In=1.48) while island shape crystals are indium–rich (Cu/In=0.68). The literature data allow for assumptions that the matrix area consists of $\text{Cu}_{11}\text{In}_9$ and that the island - type crystals consist of a CuIn_x ($x = 1, 2$) phase, the composition of which has been discussed for a long time (look for literature overview). Our EDS results (Table 3.1) give evidence of the presence of CuIn_2 that fits with results by several authors [31, 36, 39, 49, 52] about the existence of a CuIn_2 phase in sputtered Cu-In alloy films at low temperatures. The observed discrepancy of the results obtained by the EDS analysis compared with the precise ratio of Cu and In in CuInSe_2 can be explained with the small sizes of the island crystals and the matrix areas between them that are smaller than the lateral sensitivity of the EDS analysis.

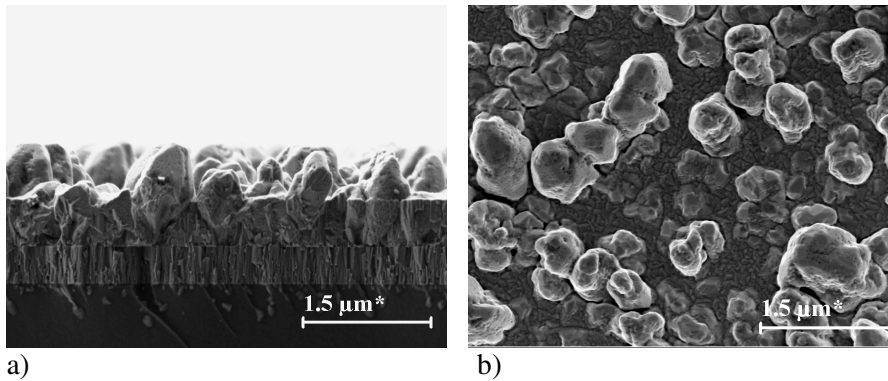


Fig. 3.1. SEM images of the surface and cross-section of the Cu-In alloy film (Cu/In=0.88). A rough bi-layer structure of the surface is well seen.

Table 3.1. Elemental composition of precursor films

	[Cu]	[In]	[Cu]/[In]	Postulated phases
Matrix area	59	41	1.48	$\text{Cu}_{11}\text{In}_9$
Island type crystals	38	62	0.63	CuIn_2

The results of the XRD analysis (Fig. 3.2a) confirm assumptions about the existence of $\text{Cu}_{11}\text{In}_9$ and CuIn_2 phases in our films. The presence of CuIn_2 in the form of island type crystals could be attributed to the high $\text{CuIn}_2/\text{Cu}_{11}\text{In}_9$ interfacial energy by [43].

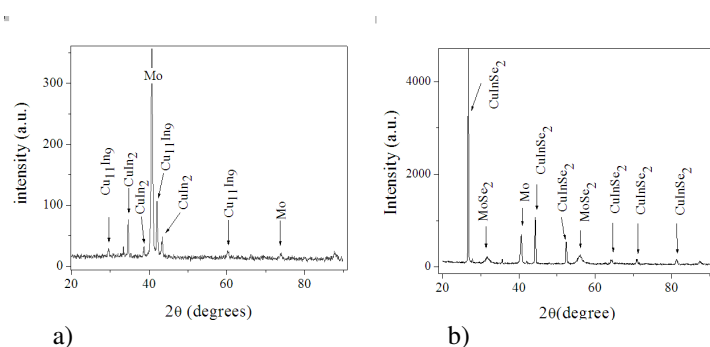


Fig. 3.2 XRD patterns of : a-the co-sputtered Cu-In alloy film. The peaks of CuIn_2 and $\text{Cu}_{11}\text{In}_9$ are revealed; b- the Cu-In film annealed at 470°C . The peaks of CuInSe_2 and MoSe_2 are revealed

3.1.2. Selenized copper and indium alloy layers

Two different experimental setups were used for selenization: a) selenization in isothermal sealed quartz ampoules, in which the Se pressure was controlled by the temperature of the selenization; b) selenization in two temperature zone sealed quartz ampoules, in which Se pressure was determined by the lower temperature zone of the ampoule. The temperature of selenization was varied from 175 to 550°C the duration of the selenization was between 0.25 and 2 hours. Se pressure was varied between 0.01 and 25 Torr.

The films selenized at temperatures up to 270°C (Fig. 3.3) show rough surface structures. The surface is characterized by relatively large crystals with sizes of up to $2\ \mu\text{m}$ and with rounded grains that are located in the small-crystalline matrix layer (with crystal sizes between 20 - 50 nm). In contrast to the alloy films here these large crystals do not extend down to the substrate Mo layer being located only on the film surface. The lower part of the selenized layers close to the Mo covered substrate consists of needle type crystals that are very different from the crystals in the matrix layer. Such a difference in the morphology of the surface and the inner structure of the layers suggests that the layers exhibit the multiphase composition. The observed

multiphase structure results from the diffusion of Cu from the bulk of alloy to the film surface, where it selenizes up to different binary copper selenides in the form of large crystal-like formations on the surface. The EDS analysis confirms that at the selenization at temperatures 270°C the composition of large crystals on the surface corresponds to the binary CuSe_2 (Table 3.2).

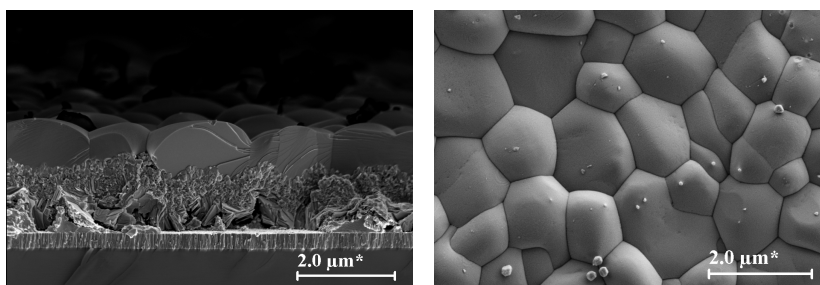


Fig. 3.3. SEM image of surface and cross-sectional Cu-In alloy film selenized at 270°C

The films selenized at 300°C (Fig. 3.4) analogously to films selenized at 270°C, show rough surface structures. Similarly, the surface is characterized by relatively large crystals (1) with sizes of up to 1 μm and with rounded grains. At the same time, in contrast to films selenized at 270°C, the EDS analysis indicates to the composition of large crystals on the surface of 300°C selenized films that corresponds to the binary CuSe (Table 3.2.). The strongest peak in Raman spectra (Fig. 3.5) at 262 cm^{-1} has been generally attributed to different binary copper selenides (CuSe_2 , CuSe , Cu_{2-x}Se) [105]. A weak peak in Raman spectra at 174 cm^{-1} is generally linked to the A_1 mode of CuInSe_2 [106]. The peaks at 114 cm^{-1} and 226 cm^{-1} indicate to the presence of InSe [107]. Results of the EDS analysis at the points 1, 2, 3 (Fig. 3.4) confirm that the formations on the surface of the layers consist of a “pure” CuSe phase and that the small-crystalline matrix is the CuInSe_2 phase with nearly stoichiometric composition, and that the needle-like crystals at the bottom represent InSe . The CuInSe_2 layer in films selenized at 300°C is thicker than in the film selenized at 270°C.

Table 3.2. Elemental composition of annealed at 300°C films

	Cu, at %	In, at %	Se, at %
Big crystals on the surface	34.3		65.7
Needle like crystals		50.6	49.4

The surface and cross-sectional SEM images indicate that the structure of the layers selenized at 330 and 370°C (Fig. 3.4b) is quite similar. However, it is very much different from that of the precursor layers and from the layers selenized at 300°C (Fig. 3.4a). The layers consist of densely packed crystals with sizes varying from 50 to 200 nm. The surface of the layers is characterized by relatively large but shallow holes and hills that could be the origin of island - like structures in the

precursor layers. The compositional sensitive EBS detector indicates a single-phase composition of the layers selenized at 375°C and the Cu/In ratio close to the initial ratio in the precursor layer. Results of XRD and Raman spectroscopy (Fig. 3.5) investigations confirm the single phase (CuInSe_2) composition of the layers.

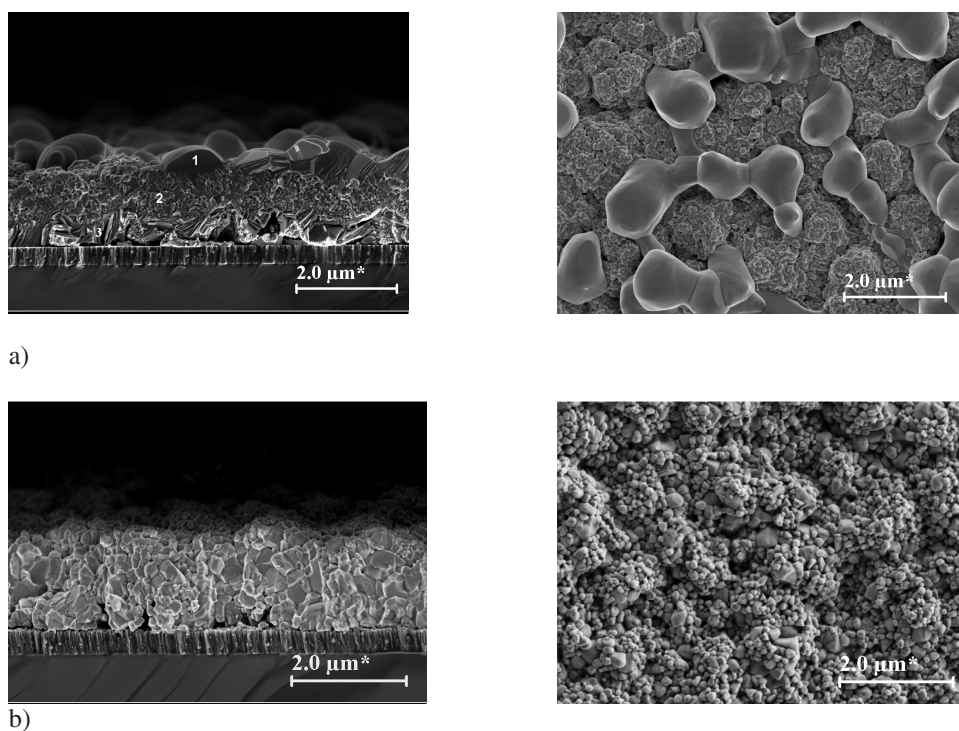


Fig. 3.4. Surface and cross-sectional images of selenized Cu-In alloy layers: a- selenization temperature 300°C; b- selenization temperature 370°C

The surface and the cross-sectional SEM images (Fig. 3.6) of layers selenized at temperatures higher than 420°C exhibit uniform, large and densely packed crystals with sizes of about 2-3 μm . The surface of the films is relatively smooth, providing good starting conditions for their use as absorber layers. Results of XRD analyses confirm that the layers selenized at 470°C were nearly single phased (Fig. 3. 2b). Micro-Raman studies revealed the existence of the InSe separate phase in very low concentrations (Fig. 3.5) that was lower than the sensitivity of EDS and XRD analyses. The results of EDS analysis indicate that the layers selenized at 470°C were homogeneous in composition, Se-rich and with the Cu/In ratio near to the Cu/In ratio of the sputtering target. The thickness of the formed well-grown CuInSe_2 films was about three times higher than that of precursor layers. The formation of MoSe_2 was detected only in completely selenized films where no intermediate binary compounds were monitored by XRD.

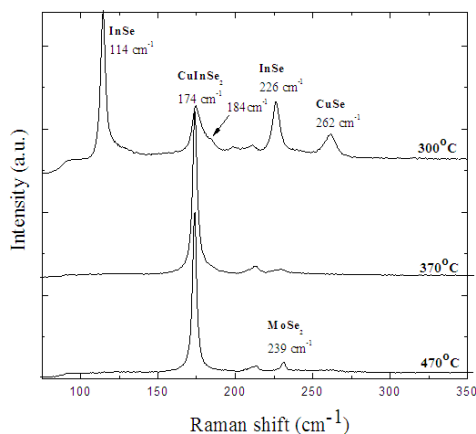


Fig. 3.5. Raman spectra of Cu-In films selenized at different temperatures

The formation of CuInSe_2 that is initiated at the temperature of 300°C , at 420°C results in films with large and densely packed crystals with sizes of about $2\ \mu\text{m}$ (Fig. 3.7b). The Cu/In ratio in the selenized films was similar to the composition of the sputtering target. This result is different from our results of the sulphurization of Cu-In alloy layers in analogous conditions (Table 3.3).

Table 3.3. Elemental composition of Cu-In films selenized and sulphurized at different temperatures

	Cu, at %	In, at %	Se (S), at %
Selenized layers, 375°C	23.5	25.5	51.0
Selenized layers, 470°C	23.6	24.6	51.8
Sulphurized layers, 470°C	26.1	24.7	49.2

Sulphurization always leads to Cu-rich films even if In-rich precursor films (Cu/In=0.88) are used. The Cu rich composition of sulphurized films could be a result of indium loss during the sulphurization process due to the formation of InS_2 with high vapour pressure already at low temperatures [108]. At the same time, indium selenides have a lower vapour pressure [42].

To summarize our results we can confirm the assumptions [109] that the formation of CuInSe_2 proceeds through three different processes. At lower temperatures the dominating processes are Se incorporation and Cu out-diffusion and the formation of different copper and indium selenides (Figs. 3.4a, 3.5). This is followed by the reaction between the binary selenides with excess Se vapour and results in the formation of CuInSe_2 (Figs. 3.4b, 3.5). The final stage is the growth of CuInSe_2 crystals leading to well-formed films with crystals of large size (Fig. 3.6).

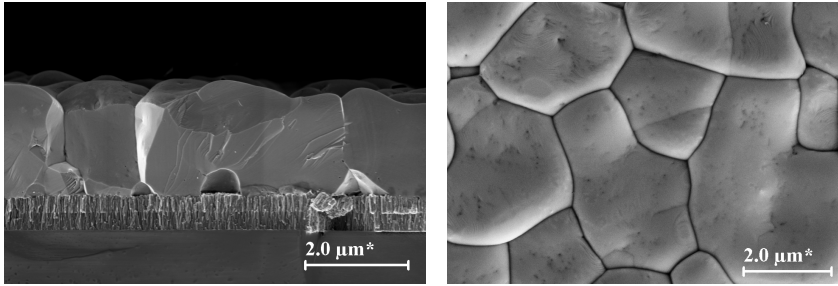


Fig. 3.6. Surface and cross-sectional images of Cu-In alloy layers selenized at the temperature 470°C

The films selenized at temperatures higher than 420°C showed preferred orientation along the (112) plane, which was enhanced by higher temperatures. The structural evolution of films in the selenization process was additionally illustrated by the increase of film thickness during the selenization process at temperatures over 370°C (Fig. 3.7).

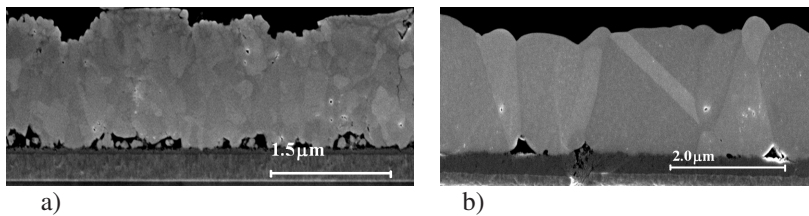


Fig. 3.7. SEM images of polished cross-sections of films selenized; a-at 370°C and b-at 420°C

The influence of the increase in the duration of selenization on the phase composition and crystal structure of films depends markedly on the selenization temperature. At low temperatures (175°C-210°C) the content of different binary selenides in samples increases with the duration of selenization. It confirms that the selenization process at low temperatures is kinetically controlled due to the insufficient amount of Se in the vapour for sample selenization. At 300°C the increase in the duration of selenization is revealed mainly in an increased content of the CuInSe_2 phase. At temperatures higher than 400°C the main effect of the increase in the duration of selenization is in accelerated recrystallization and in the increase of grain size in single-phase CuInSe_2 films.

The selenization of Cu-In alloy precursor films leads to the films with a coexistence of both chalcopyrite and Cu-Au polymorphic phases. The existence of the Cu-Au polymorphic phase in addition to the CIS phase was confirmed by the shoulder (Fig. 3.5) of chalcopyrite CIS peak at 174 cm^{-1} in Raman spectra [106] (Cu-Au phase is responsible for the peak at 183 cm^{-1} [110]). The formation of Cu-Au polymorphic CuInSe_2 phase was promoted by shorter selenization times, by lower selenization temperatures and by lower Se vapour pressures during the selenization process.

The selenization of Mo and the formation of MoSe_2 were detected at temperatures above 370°C if the complete formation of CuInSe_2 was secured. The thickness of the formed MoSe_2 layer increased remarkably with the increase of selenization temperature at the temperature range of $370\text{--}470^\circ\text{C}$ (compare Figs. 3.7a and 3.7b)

EBSD was used to study more precisely the crystal formation process in selenized films. Recording and evaluating of EBSD patterns of cross-sections of thin films selenized at different temperatures allow us to determine orientations of single grains in selenized films with respect to a reference coordinate system. The colours in the orientation maps (Figs. 3.8 and 3.9) correspond to various crystallographic directions.

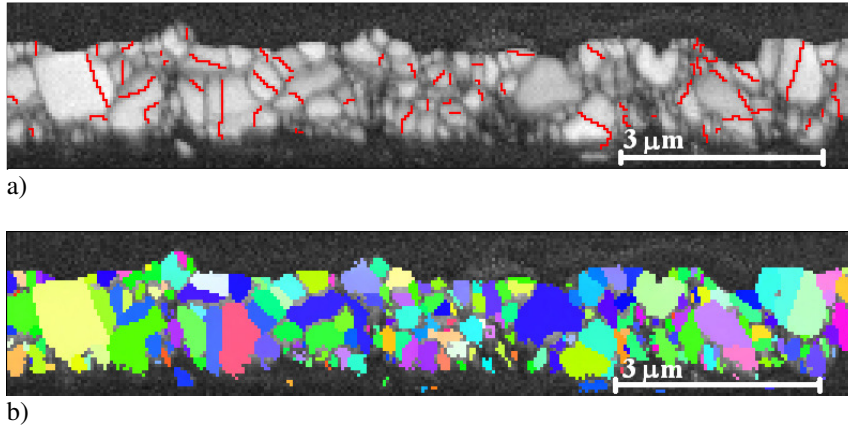


Fig. 3.8. EBSD orientation map of films selenized at 370°C

EBSD orientation map (Fig. 3.8) confirms that the films selenized at temperature 370°C are small-crystalline and consist of randomly oriented crystals. Grain sizes of the formed CuInSe_2 thin films are in the range of $50\ \text{nm}$ to $300\ \text{nm}$. Most of larger “individual” grains in the figure consist actually from several twin grains divided by twin boundaries (red lines in Fig. 3.8a). EBSD orientation maps of films selenized at 420°C (Fig. 3.9) indicate to the increase of crystal size up to $2\ \mu\text{m}$. EBSD orientation maps show the differences in the orientation of different grains in the film, in spite of the fact that XRD indicated to the preferable orientation of crystals in films indirection (112). Twin formation with an alternating orientation of adjacent grains with grain boundaries oriented (nearly) parallel to each other is clearly visible (Fig. 3.9a). The obtained results are in good coincidence with EBSD investigations of CuInS_2 and $\text{Cu}(\text{In,Ga})\text{Se}_2$ films in [111] and those of CdTe thin films in [112]. The relative frequencies of the twin boundaries in the films selenized at 370 and 470°C (not given here) were considerably larger than those in films selenized at 420°C . This allows for a conclusion that selenization at 420°C is optimal. Our results support the idea of [111] that twin formation works as a strain compensation mechanism in the selenization process, helping to compensate volume change during the formation of CuInSe_2 in films in the selenization process.

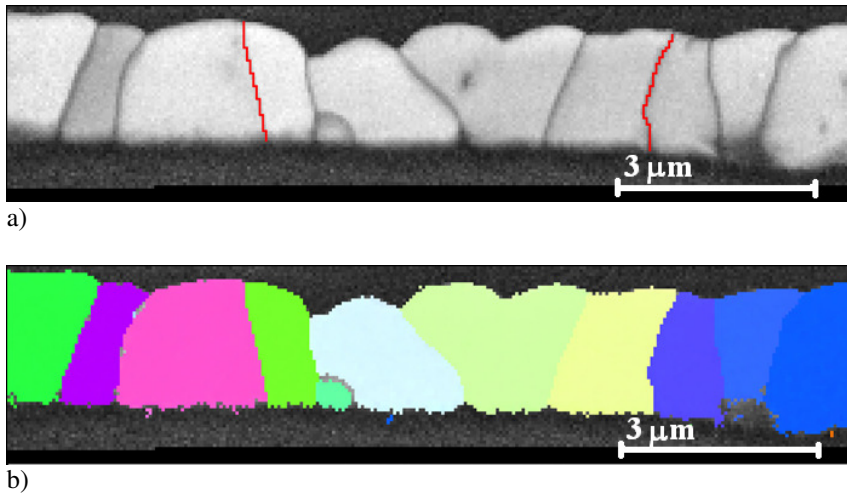


Fig. 3.9. EBSD orientation map of films selenized at 420°C

3.2. Selenization of Sn-Cu-Zn stacked layers

The results of research in this field have been published and are described in (III) in Appendix A.

R&D for the next generation photovoltaic (PV) systems strongly relies on the capability to boost pioneering technologies, including the development and use of new low-cost materials [1]. Cost reduction could be achieved by the introduction of new materials such as $\text{Cu}_2\text{ZnSnSe}_4$ (hereinafter denoted as CZTS, including also the sulphur-based compounds), which can be regarded as an alternative to CIS and CIGS materials, with the extremely expensive and resource limited Indium being replaced by cheap and abundant Zinc (Zn) and (Sn) [113]. This completely new material has yet been investigated only by very few groups and produced mainly as a thin film [114-122] by methods that, in principle, are similar to those used so far to grow CIS and CIGS layers. Quaternary CZTS thin films have been reported to have been produced by pulsed laser ablation [114, 115], RF magnetron sputtering [116, 117], co-evaporation of elements [119], sequential evaporation [120], chemical spray deposition [121], and synthesis from the melt [122]. Most of the recent studies report a conversion efficiency of 5.74% for a CZTS-based thin film solar cell obtained by sputtering and vapour phase sulphurization [120]. This figure is well below the reported best efficiencies for CIGS solar cells (up to 19% in the lab) [122], but it is encouraging as a starting point. Using monograin powders and monograin layer design of structures, efficiencies of over 5 % have been achieved [123].

Production of CZTS materials with suitable characteristics for PV application requires similar investigations to understand CZTS material formation in the chalcogenization process and to avoid the formation of secondary phases (CuSe , ZnSe , SnSe_2) and to obtain the required stoichiometry. At the same time, only very few studies have been published on the CZTS system and mainly for $\text{Cu}_2\text{ZnSnS}_4$ [83, 84, 124].

3.2.1. Sequential precursor films

The morphology of precursor films depends on the sequence of layers (Figs. 3.10 - 3.12). Precursor Sn-Zn-Cu films exhibit well formed “mesa-like” structure of the surface in which larger crystals are located on a “small-crystalline” valley (Fig. 3.10a). The size of “mesa-forming” crystals is about 1 μm . The analysis of the cross-sectional SEM images of Sn-Zn-Cu films indicates that “mesa – forming” crystals extend through the layer down to the Mo layer. The analysis of the cross-sectional SEM images and EDS data allows us to conclude that these crystals originate from the deposited Sn layer. During the Sn deposition it forms a discontinuous layer of semispherical crystals covered with several facets onto the surface of Mo substrate, leading already to the “mesa-like” structure of the Sn layer. The following depositions of Zn and Cu lead to the formation layers of these metals quite uniform in thickness on the whole surface of samples that result in a “mesa-like” structure of the surface of the final Sn-Zn-Cu films. The formation of Sn in the form of discontinuous layer of semispherical crystals could be an indication of high Sn/Mo interfacial energy.

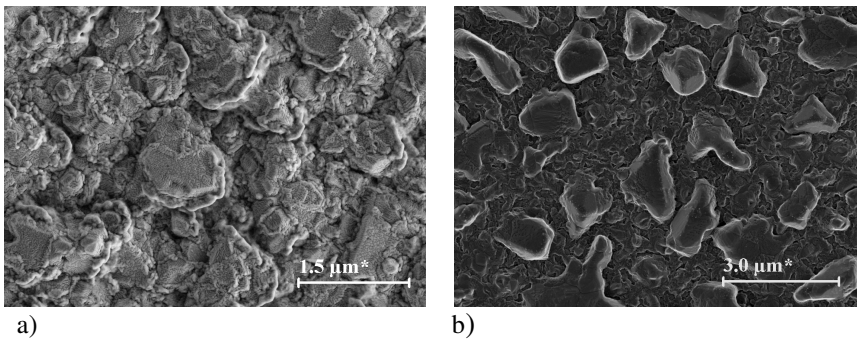


Fig. 3.10 SEM images of the surface; a- of the Sn-Zn-Cu sequential film and b- Cu-Zn-Sn sequential film

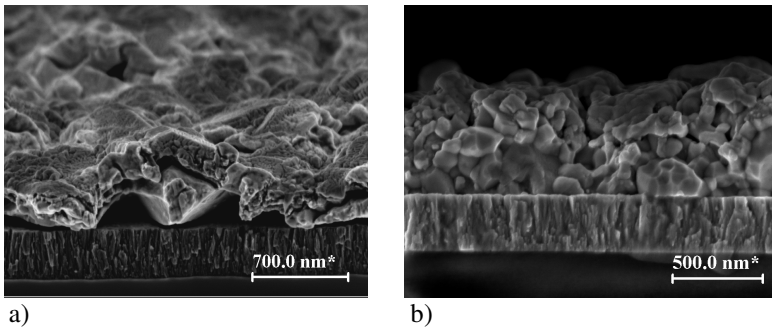


Fig. 3.11 SEM images of the cross section; a- of the Sn-Zn-Cu sequential film and b-the Cu-Zn-Sn sequential film

For films with another sequence of metallic layers, the mesa like structure is not so well exposed, and well formed flat precursor layers were produced replacing metallic layers with Cu/Sn alloy layer (Fig. 3.12). The analysis of XRD patterns gives

evidence of the existence of separate phases of Cu_5Zn_8 and Cu_6Sn_5 in the precursor Sn-Zn-Cu films (Fig. 3.13a).

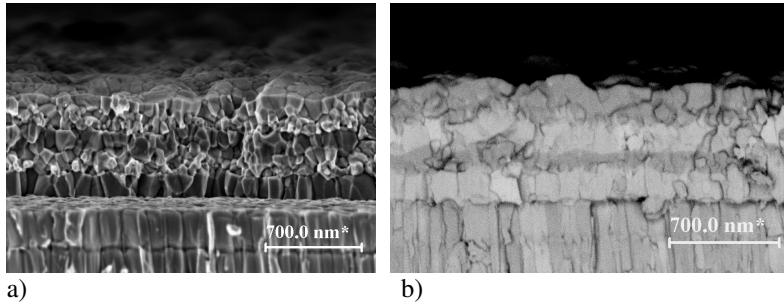


Fig. 3.12 SE SEM images (a) and EsB SEM images (b) of the cross section of the $2x(\text{Cu}/\text{Sn}-\text{Zn})$ sequential film

The results of the EDS and XRD analysis confirm that the phase Cu_6Sn_5 in the mixture of Cu_3Sn forms already in the samples produced by melting at high temperatures of elemental Cu and Sn in the ratio $2\text{Cu}+\text{Sn}$ (Fig. 3.13b).

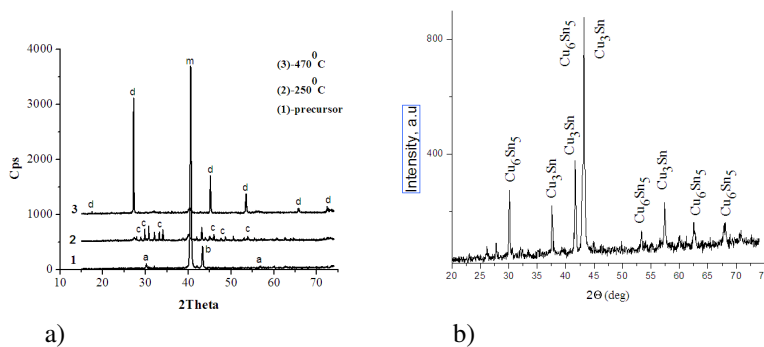


Fig. 3.13. XRD patterns of : a) precursor Sn-Zn-Sn film (1) film selenized at 250°C (2) and 470°C (3). Peaks identification: a - Cu_6Sn_5 , b - Cu_5Zn_8 , c - CuSe_2 , d - $\text{Cu}_2\text{ZnSnSe}_4$, m - Mo; b) alloy $2\text{Cu}+\text{Sn}$

3.2.2. Investigation of selenized Sn-Zn-Cu sequential films

Selenization was performed in isothermal sealed quartz ampoules, in which Se pressure was controlled by the temperature of selenization. The temperature of selenization was chosen $250, 300, 370, 420, 470,$ and 520°C , the duration of selenization varying between 20 minutes and 2 hours. The Se pressure was varied between 0.1 and 25 Torr. Methods of characterization were described in detail in section 3.

The regularities of the selenization of films of different sequence appeared quite similar. The surface of films selenized at 250°C (Fig. 3.14a) is characterized with a multiple-level structure. The upper nearly continuous layer consists of relatively large rounded grains (1, Fig. 3.14a) with sizes of up to 2 μm . The inner small-crystalline layer is composed of rounded crystals in sizes between 50-100 nm (2, Fig. 3.14a) and several plate-like crystals. In contrast to the precursor films here these large rounded crystals do not extend down to the substrate Mo layer, being located only on the surface of the films. Such morphology of the surface and inner structure of the layers suggests that the films selenized at 250°C exhibit a multi-phase composition. XRD investigations and EDS analyses refer to the presence of the CuSe_2 phase and to the additional metallic alloy phases (Cu_5Zn_8 , Cu_6Sn_5) (Fig. 3.13a) in films. The formation of copper binaries as the first step of the selenization of metallic alloy and sequential layers has been reported by different authors [45, 70, 79]. Our results are in good coincidence with literature results that at low temperatures, Cu preferably selenizes up to the formation of CuSe_2 on the surface of the layers in excess of selenium. The results of the EDS are in good compliance with the results of XRD and Raman analysis and confirm that the grains on the surface of the layers consist of a “pure” CuSe_2 phase ([Cu] = 36.6 %, [Se] = 63.4 %). The observed discrepancy of the results obtained by the EDS analysis can be explained by the small sizes of the island crystals and the matrix areas between them that are smaller than the lateral sensitivity of the EDS analysis.

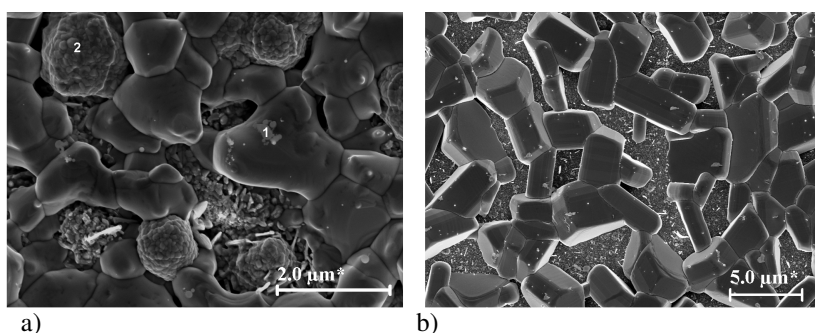


Fig. 3.14 SEM images of the surface of the Sn-Zn-Cu sequential film selenized at 250°C (a) and of the surface of the Cu/Sn-Zn sequential film selenized at 300°C (b)

The very strong peak observed in Raman spectra (Fig. 3.15) at 262 cm^{-1} is generally linked to different binary copper selenides (CuSe , Cu_{2-x}Se , CuSe_2) [105]. The peaks at 95 and 111 cm^{-1} observed in Raman spectra were detected also in the Raman spectra of alloy 2Cu+Sn. It was confirmed that the un-selenized metallic alloy (Cu_6Sn_5 on the basis of XRD analyses) is responsible for these peaks. All the results obtained give evidence that selenization at 250°C is not complete and it results in the layers of undetermined inhomogeneous structure.

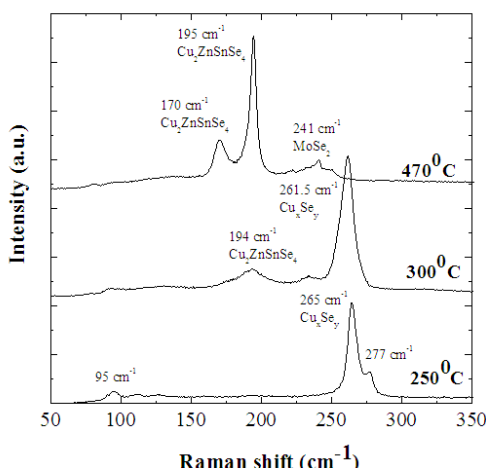


Fig. 3.15 Raman spectra of Sn-Zn-Cu films selenized at different temperatures

The films selenized at 300°C (Fig. 3.17) show similarity to the films selenized at 250°C, i.e. in their rough surface structure. The surface is covered with grains with well-formed boundaries in sizes of 1000-2000 nm. The grains are connected with necks into chains. The inner layer consists of agglomerated formations nearly in the same size. The size of crystals in agglomerates is about 30-70 nm. Raman spectra (Fig. 3.16) and XRD (Fig. 3.14) indicate to the multi-phase structure of the selenized films. Similarly to 250°C, a peak at 262 cm⁻¹ dominates in Raman spectra. In contrast to films selenized at 250°C, the EDS analysis of the films selenized at 300°C indicates that the dominating Cu binary is CuSe ([Cu] = 50.2 %, ([Se]= 49.8%). At the same time, agglomerate particles consist mainly of a mixture of ternary Cu₂ZnSnSe₃ and quaternary Cu₂ZnSnSe₄ with a small extra of a separate ZnSe phase. In the bottom layer of the films near the Mo substrate the presence of small crystals of the separate ZnSe phase was detected (Fig. 3.16a).

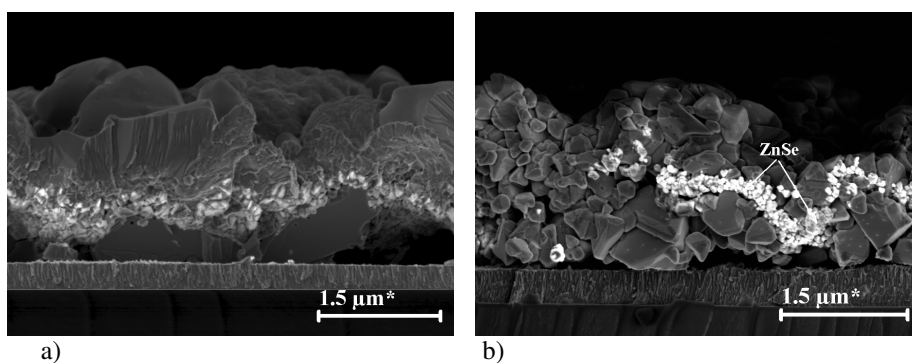


Fig. 3.16. SEM images of cross-sections of selenized at different temperatures films: a – 300°C; b-370°C

The results obtained on the dominating processes during the selenization of sequential layers at relatively low temperatures differ from those by Jimbo *et al.* [83] about the preferential sulfurization of Zn in the initial stages of the sulphurization of Cu-Zn-Sn films. Our results indicate that the selenization of Cu is dominating in any sequence of layers and binary Cu selenides in different composition are formed at low temperatures. The selenization of Cu dominates even for precursors where the Cu layer was the lowest layer (Cu-Zn-Sn). At the same time, our results are in very good compliance with the results of the chalcogenization of Cu-In layers [5, 44, 45, 49, 70].

The reticulate surface structure of films selenized at 370°C (Fig. 3.17a) differs significantly from that selenized at lower temperatures. The surface of the films consists of large agglomerated rounded grains (Fig. 3.17a, point1) and smaller triangle-like crystals in sizes of 50-100 nm (Fig. 3.17a, point2). The considerable differences in the size and shape of the crystals in films could refer to differences in their phase composition. In addition to the CZTS phase, the results of Raman analysis indicate to the presence of separate phases of Cu_2SnSe_3 [122], SnSe_2 [125] ZnSe [126], and Cu_xSe in smaller quantities. EDS confirms that the composition of larger crystals corresponds to the CZTS and indirectly indicates that triangle-like crystals consist of the Cu_2SnSe_3 phase.

Cross-sectional SEM images (Fig. 3.18b) indicate that the structure of the layers selenized at higher than 420°C is different from that of the precursor layers and of layers selenized at lower temperatures. The films retain a two-level structure; sparse packed “large” crystals in sizes of up to 1 μm as the surface layer and dense small-crystalline bottom layer with sizes of crystals varying from 50 to 200 nm as a lower layer. The results of micro-Raman and XRD investigations confirm that in addition to dominating CZTS phase, films contain smaller quantities of phases of SnSe_2 , ZnSe and MoSe_2 [127] (Fig. 3.15, 3.13). The composition sensitive EsB detector indicates a single-phase composition of “large” crystals and the EDS shows that the ratio of elements is close to the initial ratio of elements in the precursor film.

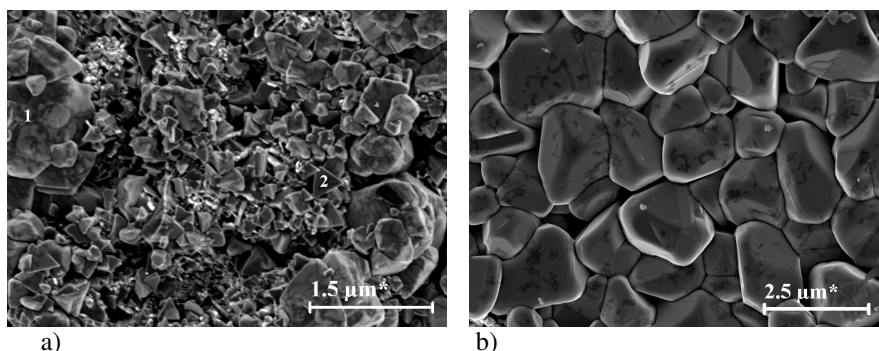


Fig. 3.17 SEM images of the surface of the stoichiometric composition films selenized at different temperatures: c-at 370°C and d-at 470°C

The surface (Figs. 3.17b, 3.18a) and the cross-sectional SEM images (Fig. 3.18b) of films selenized at 470°C exhibit homogeneous large crystals with sizes of about 2-3 μm . Our results did not give evidence of the acceleration of crystal growth

in the use of Cu-rich precursor layers, in spite of the fact that Cu_xSe crystals in the bulk and on the surface of films from Cu-rich precursors are well seen on SEM images of these materials (Figs. 3.18 a, b).

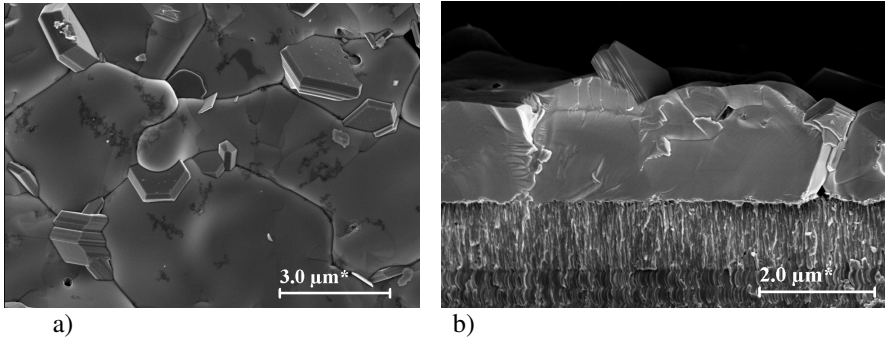


Fig. 3.18. SEM images of the surface (a) and the cross-section (b) of the Cu rich precursor films selenized at 470°C

The surface of the films is relatively smooth, providing good starting conditions for their use as absorber layers. Results of both micro-Raman and EDS spectra analyses confirm that films selenized at 470°C consist of the dominating CZTS phase and phases of ZnSe and MoSe_2 in smaller quantities similar to the films selenized at 420°C (Figs. 3.13, 3.15). The existence of a separate SnSe_2 phase was detected only by micro-Raman. It indicates that the concentration of SnSe_2 was lower than the sensitivity of EDS and XRD analyses or that the distribution of the SnSe_2 phase in films is inhomogeneous. Similarly to the films selenized at lower temperatures, a separate ZnSe phase was easily detected on the SEM images of the cross-sections of the films (Fig. 3.16b).

The formation of MoSe_2 was detected in all samples selenized at temperatures higher than 370°C . Problems of insufficient adhesion of the formed films due to the formation of a discontinuous layer of semispherical crystals of Sn in the process of deposition of precursor films did not allow us to determine the real level of Mo selenization.

To summarize, it could be concluded that the pathway to form the $\text{Cu}_2\text{ZnSnSe}_4$ phase under pressure of elemental Se and the phase composition of selenized films depends on the temperature of selenization and is relatively independent of the sequence of metallic layers in stacked films. Selenization begins always with the formation of binary Cu-selenides with compositions varying with the temperature. The selenization at temperatures higher than 370°C results in multi-phase films consisting of high quality $\text{Cu}_2\text{ZnSnSe}_4$ crystals with sizes of up to $2\ \mu\text{m}$ and of separate phase of ZnSe. The content of ZnSe diminishes with the rise of the selenization temperature, but the selenized films stayed always multi-phased.

3.3. Selenization of electrodeposited layers

As it was pointed out in the literature overview, the electrodeposition of CuInSe_2 layers differs from the classical vacuum based processes mainly by the way

the absorber is prepared. At the same time, this difference leads to several peculiarities in phase composition, stoichiometry and electrophysical parameters of CuInSe_2 layers. Structural, electrical and optical properties of electrochemically deposited layers are by far less controlled and different additional thermal treatments are needed to obtain layers with desired properties. In the following our results of thermal treatments of different electrochemically deposited precursor layers in different atmospheric conditions will be given.

3.3.1. Influence of annealing conditions on the structural quality of CuInSe_2 thin films

The results of research in this field have been published and are described in IV in Appendix A.

Precursor films. Morphology and composition of one step electrodeposited films depend on the deposition potential and on the ratio of In and Cu in initial solutions. CIS precursor layers with thickness about $1\ \mu\text{m}$ were prepared by one step electrochemical deposition from aqueous solutions. Preliminary experiments indicate that deposition at low values of deposition potential lead to dense, smooth films (Fig. 3.19a). The films are polycrystalline by nature and contain additional phases such as different selenides of copper and indium and elementary selenium [103]. The CuInSe_2 films deposited at high values of the deposition potential were in dendritic, porous structure (Fig. 3.19b). At the same time, the summary elemental composition of a film was independent of the deposition potential (of film morphology). In our research mainly compact, precursor films with uniform composition and adherent to the substrate were used as precursors (Fig. 3.19a). The overall chemical composition of the electrodeposited precursor CIS layers determined by the EDX was slightly Cu-rich ($\text{Cu}:\text{In}:\text{Se} = 25:23:52$).

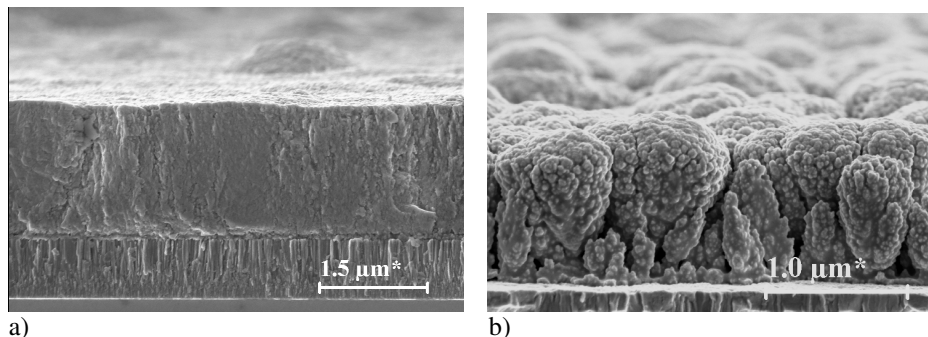


Fig. 3.19. SEM images of cross-sections of electrodeposited CIS thin films

Thermal treatment under Se vapour. The structural evolution of layers in the Se annealing process is illustrated as SEM images of annealed films (Figs. 3.20a, 3.21). The grain size increases in annealing process. The films consist of relatively large grains in the range of 400–700 nm and single grains that extend through the whole film thickness. The annealed films exhibit a high density of extended defects

such as faceted voids, pores and inclusions of other phases (Fig. 3.20a). The thickness of annealed CuInSe_2 films was less by 1/3 of the thickness of as-deposited precursor films that indicates to the intense recrystallisation during annealing. Average bulk composition determined from EDS measurements did not change noticeably in thermal annealing process and was slightly Cu-rich or near to stoichiometric. The XRD patterns of thermally treated samples (Fig.3.22) show diffraction peaks corresponding to chalcopyrite CuInSe_2 with (112) as main reflection.

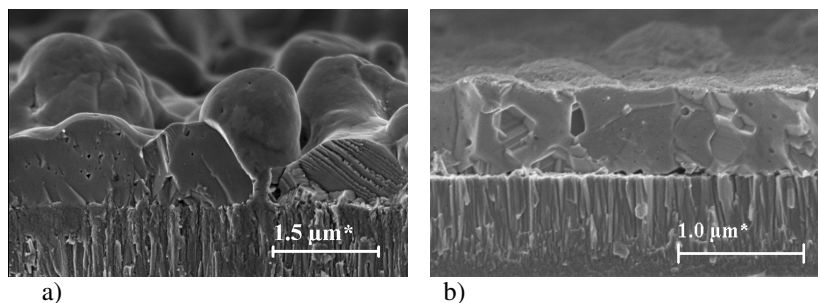


Fig. 3.20 SEM images of cross-section of CIS films: a-annealed under Se vapour pressure 10 Torr. Temperature of annealing at 450°C, duration 30 min. b- annealed in vacuum. Temperature of annealing 450°C, duration 30 min

An analysis of selenized films using the EsB detector exposes crystalline areas different in structure and composition (Fig. 3.21). The image reveals a matrix homogeneous and uniform CIS regions (1), island regions (3) with large In-rich CIS grains and the Cu–Se phase (2) segregated to the bottom layer. The segregation of Cu–Se phases to the bottom of CIS films was clearly seen at cross-sectional images of the Cu- rich CIS film ($\text{Cu}/\text{In}=1.5$) and on the EDS profiles of elements in cross-sections (Fig. 3.23). The comparison of results of Raman and SEM investigations provides a basis for a conclusion that in annealed Cu-rich CIS films a Cu–Au type structure (CA) is coexisting with its embedding chalcopyrite (CH) CIS structure (Figs. 3.23a and 3.24).

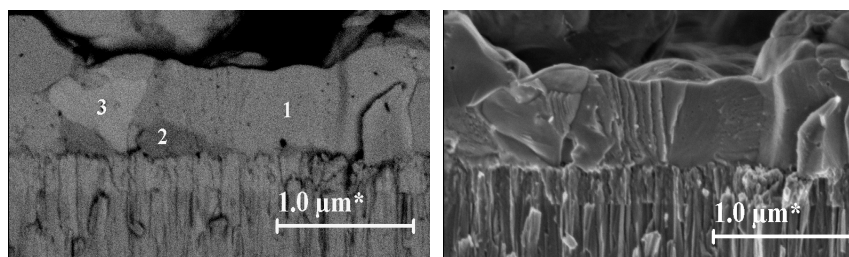


Fig. 3.21 EsB and SE SEM images of the cross-section of CIS thin film annealed under selenium vapour pressure of 1 Torr at 450°C

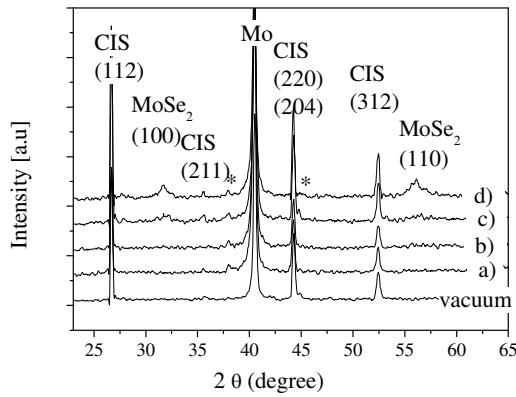


Figure 3.22 XRD patterns of CIS films annealed under different Se vapour pressure: a- 0.001 Torr, b- 0.01 Torr, c- 1 Torr, d- 10 Torr, and at dynamic vacuum 10^{-3} Torr. (* - MoSe_2)

The formation of MoSe_2 interlayer was observed in films thermally treated in selenium atmosphere as a result of Se diffusion through the CIS film and the following reaction with the Mo back contact layer. The formed MoSe_2 layer was clearly seen on the SEM image (Fig. 3.21) and its existence was confirmed additionally by the XRD analysis (Fig. 3.22) and on EDS scanning profile (Fig. 3.23b). The thickness of the MoSe_2 layer grows with the Se vapour pressure increasing; at Se pressure 0.01 Torr it was 30 nm, at Se pressure 1 Torr about 200 nm and at Se pressure about 10 Torr the thickness of the MoSe_2 layer was about 300 nm.

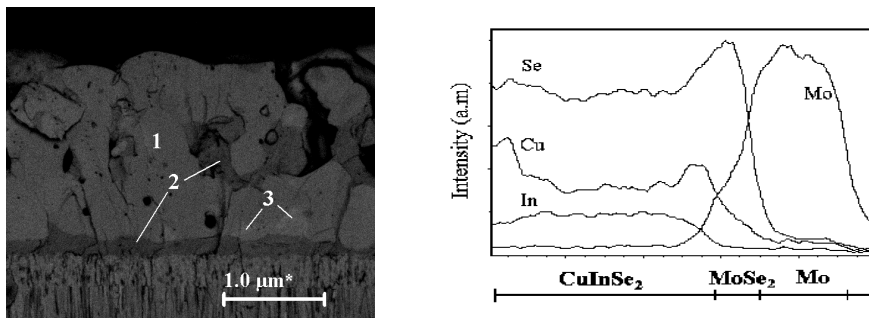


Fig. 3.23. EsB image (a) and EDS line scanning profile (b) of the cross-section of a Cu-rich CIS film grown at 450°C under selenium vapour pressure 10 Torr

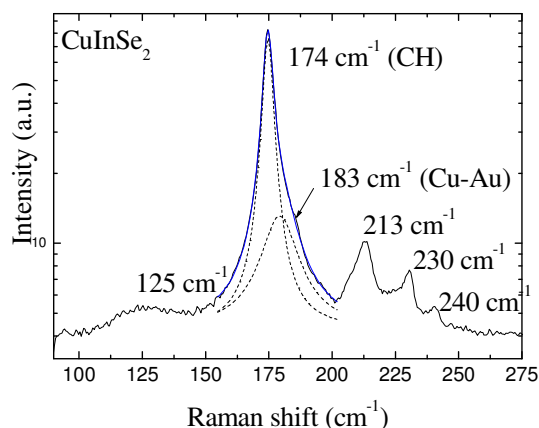


Fig. 3.24. Raman spectra of CuInSe₂ annealed at 450°C under selenium vapour pressure 10 Torr

Thermal treatment in vacuum. The structure of films annealed in dynamic vacuum (at the equilibrium Se pressure of dissociation of CuInSe₂ about 10⁻⁴ Torr) seems to be more nanocrystalline (crystal sizes about 50 nm) comparing with Se vapour pressure treated films (Fig. 3.25). The SEM EsB images expose the non-homogeneous structure with a fragmentary inclusion of Cu-rich phases different in size and composition. The inclusions of a Cu-rich region (4) in bulk matrix (2) are well seen. The thickness of the films was reduced by up to one third (initial thickness of films was 1.5 μm) as a result of an increase in the density of the reacted film and, perhaps, as a result of some loss of material during the annealing process during annealing. The EsB image reveals the exfoliation of the film. The fine-grained layer with a thickness of about 30 nm (1) covers the surface of the CIS film. The composition of this upper layer has deficiency in copper. The dark grains (3) that are formed on the bottom of CIS films correspond to the Cu-Se phase recrystallized during vacuum annealing. The formation of MoSe₂ interlayer was not observed even after a six-hour annealing in vacuum. Very long durations of annealing (up to 12h) lead to the loss of Se and In, as indicated in Table 3.4.

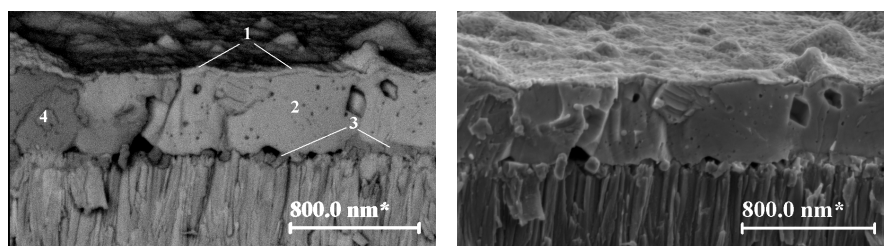


Figure 3.25. EsB and SE images of the cross-section of a Cu-rich electrodeposited CIS film annealed in vacuum at 450°C during 6 hours

Table 3.4. Composition of vacuum annealed electrodeposited CIS thin films

Duration of annealing , h	Cu, at%	In, at%	Se, at%
As-deposited	25	23	52
0.25	30	22.6	47.4
0.5	29.4	22.3	48.3
1	27.5	21.8	50.5
3	32.3	22	45.7
6	32.5	21.2	46.3
12	46	23.8	30.2

CONCLUSIONS

The results of the thesis could be summarized in the conclusions as follows:

1. SEM investigation is powerful method in research of complicated compound materials for solar energetics
2. The formation of CuInSe_2 and $\text{Cu}_2\text{ZnSnSe}_4$ films in selenization process proceeds through three different stages:
 - at lower temperatures the dominating processes are Se incorporation and Cu out-diffusion and the formation of different copper and indium selenides.
 - this is followed by the reaction between the binary selenides with excess Se vapour and results in the formation of CuInSe_2 and $\text{Cu}_2\text{ZnSnSe}_4$
 - the final stage is the growth of CuInSe_2 and $\text{Cu}_2\text{ZnSnSe}_4$ crystals leading to well-formed films with crystals of large size .
3. The pathway of formation of the CuInSe_2 and $\text{Cu}_2\text{ZnSnSe}_4$ phases during the selenization of alloy and sequential films under the pressure of elemental Se is kinetically controlled and the phase composition of selenized films depends on the temperature of selenization.
- 4 . Only selenization at high temperatures (higher than 420°C) results in high quality dense chalcopyrite CuInSe_2 films with crystals of about $2\ \mu\text{m}$ and with a preferred orientation of the crystals in the (112) direction. The formation of MoSe_2 layer was observed only if the formation of CuInSe_2 phase was completed and no separate binary phases were found in selenized layers.
5. The selenization of Sn-Zn-Cu films under the pressure of elemental Se at temperatures higher than 400°C results always in multiphase films that consist of high quality $\text{Cu}_2\text{ZnSnSe}_4$ crystals with a size of about $2\ \mu\text{m}$ and of an additional separate phase of ZnSe.
6. The recrystallization processes in the electrodeposited CuInSe_2 thin films depend on the Se vapour pressure and precursor film composition. The diffusion of elements in the CIS film matrix leads to the accelerated recrystallization of CuInSe_2 . The formation of MoSe_2 interlayer was observed only in the samples thermally treated in the selenium atmosphere.

REFERENCES

1. A vision of photovoltaic technology for 2030 and beyond, European Commission, 2004.
2. Handbook of Photovoltaic Science and Engineering /A. Luque, S.Hegedus (editors). Wiley, 2006. 1138p.
3. J.I. Goldstein, D.E. Newbury, P. Echlin, D.C. Joy, C.E. Lyman, E. Lifshin, L.Sawyer, J.R. Michael. Scanning Electron Microscopy and X-Ray Microanalysis. New York: Kluwer Academic/Plenum Publishers, 2003. 689 p.
4. A. Goetzberger, C. Hebling, H.-W. Schock. Photovoltaic materials, history, status and outlook.- Materials Science and Engineering , 2003, R 40, p. 1-46.
5. Scanning Microscopy for Nanotechnology/ W. Zhou, Z. L.Wang (editors). Springer, 2007. 522 p.
6. R.F. Egerton. Physical Principles of Electron Microscopy. Springer, 2005. 202 p.
7. D. Brandon, W. D. Kaplan. Microstructural Characterization of Materials. Wiley, 2006. 550 p.
8. H. Moutinho, R. Dhere, C.-S. Jiang, B.To, M. Al-Jassim. Electron – Backscattering Diffraction of Photovoltaic Thin Films. - Materials Research Society Symposium Proceedings 1012: Materials Research Society, 2007, Y12-04.
9. P. Kuisma-Kursula. Accuracy, Precision and Detection Limits of SEM–WDS, SEM–EDS and PIXE in the Multi-Elemental Analysis of Medieval Glass. - X-Ray Spectrum, 2000, 29, p. 111–118.
10. I. M. Kötschau, A. Weber, P. Pistor, I. Lauer mann, Ch.-H. Fischer, H.W. Schock. Advanced X-ray methods for chalcogenide thin film analysis. - Thin Solid Films, 2007, 515, p. 5992–5996.
11. J. Müller, J. Nowoczin, H. Schmitt. Composition, structure and optical properties of sputtered thin films of CuInSe₂. - Thin Solid Films, 2006, 496, p. 364-370.
12. M. Klenk, O. Schenker, U. Probst, E. Bucher. X-ray fluorescence measurements of thin film chalcopyrite solar cells. - Solar Energy Materials and Solar Cells, 1999, 58, p. 299-319.
13. A. Goetzberger, C. Hebling. Photovoltaic materials, past, present, future. - Solar Energy Materials and Solar Cells, 2000, 62, p. 1-19.
14. T. Haalboom, T. Gödecke, F. Ernst, M. Rühle, R. Herberholz, H.-W. Schock. Phase relation and microstructure in bulk materials and thin films of the ternary system Cu-In-Se. - Proceedings of the 11th International Conference on Ternary and Multinary Compounds: Salford, 1998, p. 249-252.
15. N. Rega, S. Siebentritt, I. Beckers, J. Beckmann, J. Alberts, M. Lux-Steiner. Defect spectra in epitaxial CuInSe₂ grown by MOVPE. - Thin Solid Films, 2003, 431-432, p. 186-189.
16. S. Niki, A. Yamada, R. Hunger, P. J. Fons, K. Iwata, K. Matsubara, A. Nishio and H. Nakanishi. Molecular beam epitaxial growth and characterization of

- CuInSe₂ and CuGaSe₂ for device application. - Journal of Crystal Growth, 2002, 237-239, p. 1993-1999.
17. K. Yoshino, A. Fukuyama, H. Yokoyama, K. Meada, P.J. Fons, A. Yamada, S. Niki, T. Ikai. Piezoelectric photoacoustic spectra of CuInSe₂ thin film grown by molecular beam epitaxy. - Thin Solid Films, 1999, 343-344, p. 591-593.
 18. A. A. S. Akl, A. Ashour, A. A. Ramadan, K. Abd El-Hady. Structural study of flash evaporated CuInSe₂ thin films. - Vacuum, 2001, 61, p. 75-84.
 19. M. Bodegard, O. Lundberg, J. Lu, L. Stolt. Re-crystallization and interdiffusion in CGS/CIS bilayers. - Thin Solid Films, 2003, 431-432, p. 26-30.
 20. G. Hanna, J. Mattheis, V. Laptev, Y. Yamamoto, U. Rau, and H. W. Schock. Influence of the selenium flux on the growth of Cu(In,Ga)Se₂ thin films. - Thin Solid Films, 2003, 431-432, p. 31-36.
 21. D. Lincot. Electrodeposition of semiconductors. - Thin Solid Films, 2005, 487, p. 40-48.
 22. J. Bekker, V. Alberts, A.W.R. Leitch, J.R. Botha. Properties of CuIn(Se,S)₂ thin films prepared by two-step growth processes. - Thin Solid Films, 2003, 431-432, p. 116-121.
 23. K. Ellmer, J. Hinze, J. Klaer. Copper indium disulfide solar cell absorbers prepared in a one-step process by reactive magnetron sputtering from copper and indium targets. - Thin Solid Films, 2002, 413, p. 92-97.
 24. R. Caballero and C. Guillén. CuInSe₂ formation by selenization of sequentially evaporated metallic layers. - Solar Energy Materials and Solar Cells, 2005, 86, p. 1-10.
 25. S. I. Castaneda, F. Rueda. Differences in copper indium selenide films obtained by electron beam and flash evaporation. - Thin Solid Films, 2000, 361-362, p. 145-149.
 26. S. Merdes, L. Bechiri, Z. Hadjoub, M. Sano, S. Ando. Influence of selenization temperature on the properties of CuInSe₂ thin films prepared by spin coating technique. - physica status solidi (c), 2006, 3, p. 2535-2538.
 27. M. Kaelin, H. Zogg, A. N. Tiwari, O. Wilhelm, S. E. Pratsinis, T. Meyer, A. Meyer. Electro sprayed and selenized Cu/In metal particle films. - Thin Solid Films, 2004, 457, p. 391-396.
 28. F. Jiang, J. Feng. Effect of temperature on selenization process of metallic Cu-In alloy precursors. - Thin Solid Films, 2006, 515, p. 1950-1955.
 29. J. Bekker, V. Alberts, M. J. Witcomb. Influence of selenization techniques on the reaction kinetics of chalcopyrite thin films. - Thin Solid Films, 2001, 387, p. 40-43.
 30. A. Ashour, A. A. Akl, A. A. Ramadan, K. Abd El-Hady. Electrical properties of stacked CuInSe₂ thin films. - Journal of Materials Science: Materials in Electronics, 2005, 16, p. 599-602.
 31. M. Gossila, H. Metzner, H.-E. Mahnke. Coevaporated Cu-In films as precursors for solar cells. - Journal of Applied Physics, 1999, 86, p. 3624-3632.

32. N. Orbey, H. Hichi, R. W. Birkmire, T. W. F. Russell. Effect of temperature on copper indium selenization. - Progress in photovoltaics: research and application, 1997, 5, p. 237-247.
33. C. H. Chung, S. D. Kim, H. J. Kim, F. O. Adurodija, K. H. Yoon, J. Song. Phase formation and control of morphology in sputtered Cu-In alloy layers. - Solid State Communications, 2003, 126, p. 185-190.
34. M. A. Contreras, B. Egaas, K. Ramathan. Progress towards 20% efficiency in Cu(In, Ga)Se₂ polycrystalline thin film solar cells. - Progress in Photovoltaic, 1999, 7, p. 311-316.
35. F. O. Adurodija, J. Song, K. H. Yoon, S. K. Kim, S. D. Kim, S. H. Kwon, B. T. Ahn. Preparation of CuInSe₂ thin films by selenization of co-sputtered Cu-In precursors. - Journal of Materials Science: Materials in Electronics, 1998, 9, p.361-366.
36. T. Nakano, S. Sato, S. Baba. Structural analysis of Cu-In alloy films by XPS depth profiling by ion etching. - Vacuum, 2004, 74, p. 591-594.
37. K. A. Lindahl, D. L. Olson, J. J. Moore, A. B. Swartzlander, R. Noufi. Quantitative investigation of reactions in copper-indium-gallium multilayer thin films. - Conference Record of the Twenty Fifth IEEE Photovoltaic Specialists Conference, 1996, p.949 – 952.
38. T. Nakano, T. Suzuki, N. Ohnuki, S. Baba. Alloying and electrical properties of evaporated Cu-In bilayer thin films. - Thin Solid Films, 1996, 334, p. 192-195.
39. T. Nakano, H. Mizuhashi, S. Babu. Transition of Roughness evolution in Cu-In alloy films by the formation of intermetallic compounds. - Japanese Journal of Applied Physics, 2005, 44, p.1932-1938.
40. D. Wolf, G. Müller. Kinetics of CIS-formation studied in situ by thin film calorimetry - Thin Solid Films, 2000, 361-362, p. 155-160.
41. S. Bandyopadhyaya, S. Roy, S. Chaudhuri, A.K. Pal. CuIn(S_xSe_{1-x})₂ films prepared by graphite box annealing of Cu/In stacked elemental layers. - Vacuum, 2001, 62, p. 61-73.
42. F. O. Adurodija, J. Song, S. D. Kim, S. H. Kwon, S. K. Kim, K.H. Yoon, B.T. Ahn. Growth of CuInSe₂ thin films by high vapour Se treatment of co-sputtered alloy in a graphite container. - Thin Solid Films, 1999, 338, p. 13-19.
43. C.H. Chung, S.D. Kim, H.J. Kim, F.O. Adurodija, K.H. Yoon, J. Song. Phase formation and control of morphology in sputtered Cu-In alloy layers. - Solid State Communications, 2003, 126, p. 185-190.
44. T. Pisarkiewicz, H. Jankowski. Vacuum selenization of metallic multilayers for CIS solar cells. - Vacuum, 2003, 70, p. 435-438.
45. W.K. Kim, E.A. Payzant, S. Yoon, T. J. Anderson. In situ investigation on selenization kinetics of Cu-In precursor using time-resolved, high temperature X-ray diffraction. - Journal of Crystal Growth, 2006, 294, p. 231-235.
46. G. Zoppi, I. Forbes, P. Nasikkar, R. Miles. Physical properties of CuAl_{1-x}In_xSe₂ produced by selenization of Cu/Al/In(Se) precursor layers. - 21st

- European Photovoltaic Solar Energy Conference: Dresten, Germany, 2006, p.1998-2001
47. G. Zoppi, I. Forbes, P. Nasikkar, R. W. Miles, Characterisation of thin films $\text{CuIn}_{1-x}\text{Al}_x\text{Se}_2$ Prepared by Selenisation of magnetron Sputtered Metallic Precursors. - Materials Research Society Symposium Proceedings 1012: Materials Research Society, 2007, Y12-02
 48. A. Ihlal, K. Bouabid, D. Soubane, M. Nya, O. Ait-Taleb-Ali, Y. Amira, A. Outzourhit, G. Nouet. Comparative study of sputtered and electrodeposited $\text{CuIn}(\text{S},\text{Se})$ and CuInSe_2 thin films. - Thin Solid Films, 2007, 515, p. 5852–5856.
 49. A. Brummer, V. Honkimäki, P. Berwian, V. Probst, J. Palm, R. Hock. Formation of CuInSe_2 by the annealing of stacked elemental layers – analysis by in situ high-energy powder diffraction. - Thin Solid Films, 2003, 437, p. 297–307.
 50. P. Berwian, A. Weimar, G. Müller. In situ resistivity measurements of precursor reactions in the Cu-In-Ga system. - Thin Solid Films, 2003, 431 – 432, p. 41–45.
 51. Ch. von Klopmann, J. Djordjevic, R. Scheer. Real-time study of phase transformations in Cu-In-Se-S thin films: 1. Intermetallic phase transformations. - Journal of Crystal Growth, 2006, 289, p. 113–120.
 52. E. Rudigier, J. Djordjevic, C. von Klopmann, B. Barcones, A. Perez-Rodriguez R. Scheer. Real-time study of phase transformations in Cu-In chalcogenide thin films using in situ Raman spectroscopy and XRD. - Journal of Physics and Chemistry of Solids, 2005, 66, p. 1954–1960.
 53. M. Tanda, S. Manaka, A. Yamada, M. Konagai, K. Takahashi, Japanese Journal of Applied Physics, 1993, 32, 1913-1918.
 54. S.T. Lakshmikummar, A. C. Rastorgi. Selenization of Cu and In thin films for the preparation of selenide photo-absorber layers in solar cells using Se vapour source. - Solar Energy Materials and Solar Cells, 1994, 32, p.7-19.
 55. D. Bhattacharyya, I. Forbes, F. O. Adurodija, M. J. Carter. Formation of CuInSe_2 by the selenization of sputtered Cu/In layers. - Journal Materials Science, 1997, 32, p. 1889-1894.
 56. F.O. Adurodija, J. Song, I. O. Asi, K.H. Yoon. Formation of $\text{CuIn}(\text{S},\text{Se})_2$ thin film by thermal diffusion of sulphur and selenium vapour into Cu-In alloy within a closed graphite container. - Solar Energy Materials and Solar Cells, 1999, 58, p. 287-297.
 57. H. Matsuhita, T. Takizawa. Phase diagram of the CuIn-2Se system for CuInSe_2 crystal growth by controlling Se contents. - Journal of Crystal Growth, 1997, 179, p.503-509.
 58. J. Bekker, V. Alberts, M. J. Witcomb. Influence of selenization techniques on the reaction kinetics of chalcopyrite thin films. - Thin Solid Films, 2001, 387, p. 40-43.
 59. R.Caballero, C.Guillen. Optical and electrical properties of $\text{CuIn}_{1-x}\text{Ga}_x\text{Se}_2$ thin films obtained by selenization of sequentially evaporated metallic layers. - Thin Solid Films, 2003, 431 –432, p. 200–204.

60. R. Caballero, C. Maffiotte, C. Guillen. Preparation and characterization of $\text{CuIn}_{1-x}\text{Ga}_x\text{Se}_2$ thin films obtained by sequential evaporations and different selenization processes. - *Thin Solid Films*, 2005, 474, p. 70–76.
61. E.P. Zaretskaya, V.F. Gremenok, V. Riede, W. Schmitz, K. Bente, V.B. Zalesski, O.V. Ermakov. Raman spectroscopy of CuInSe_2 thin films prepared by selenization. - *Journal of Physics and Chemistry of Solid*, 2003, 64, p. 1989-1993.
62. A. Ashour, A.A.S. Akl, A.A. Ramadan, K. Abd El-Hady. Study of polycrystalline CuInSe_2 thin film formation. - *Thin Solid Films*, 2004, 467, p. 300–307.
63. A. Ashour, A.A.S. Akl, A.A. Ramadan, N.A. El-Kadry, K.Abd El-Hady. Optical manipulation of temperature formation of CuInSe_2 thin films. - *Materials Science and Engineering*, 2006, B 134, p. 63–67.
64. X. Chuan-Ming, S. Yun, Z. Lin, L. Feng-Yan, Z. Li, X. Yu-Ming, Z. Zhi-Qiang, H. Qing. Preparation of $\text{Cu}(\text{In}, \text{Ga})\text{Se}_2$ thin film solar cells by selenization of metallic precursors in Ar atmosphere. - *Chinese Physics Letters*, 2006, 23, p. 2259-2261.
65. F.D. Jiang, L. Zhang, J.Y. Feng. Structural properties of CuInSe_2 films prepared by selenization of metallic precursors on MoN_x film substrates. - *Applied Surface Science*, 2006, 252, p. 3051-3057.
66. V. Alberts, M. L. Chenene. In – depth compositional uniformity of CuInSe_2 prepared by two – stage growth sequences. - *Journal of Physics D: Applied Physics*, 1999, 32, p. 3093-3098.
67. M. Klenk, O. Schenker, V. Alberts, E. Bucher. Control of two – step growth processes of chalcopyrite thin films by X-ray fluorescence spectroscopy. - *Applied Surface Science*, 2001, 173, p. 62-68.
68. W.K. Kim, E.A. Payzant, T. J. Anderson, O. D. Crisalle. In situ investigation of the selenization kinetics of Cu- Ga precursors using time resolved high – temperature X-ray diffraction. - *Thin Solid Films*, 2007, 515, p. 5837–5842.
69. W. K. Kim, E. A. Payzant, T. J. Anderson, O.D. Crisalle. In-situ observation of selenization of Cu-Ga-In metallic precursors.- *Conference Record of the 2006 IEEE 4th World Conference on Photovoltaic Energy Conversion, WCPEC-4*, 2007, p. 453-456.
70. F. Hergert, R. Hock, A. Weber, M. Purwins, J. Palm, V. Probst. In situ investigation of the formation of $\text{Cu}(\text{In},\text{Ga})\text{Se}_2$ from selenized metallic precursors by X-ray diffraction – The impact of Gallium, Sodium and Selenium excess. - *Journal of Physics and Chemistry of Solids*, 2005, 66, p. 1903–1907.
71. M. Purwins, A. Weber, P. Berwian, G. Müller, F. Hergert, S. Jost, R. Hock. Kinetics of the reactive crystallization of CuInSe_2 chalcopyrite films for solar cell applications. - *Journal of Crystal Growth*, 2006, 287, p. 408–413.
72. S. Jost, F. Hergert, R. Hock, M. Purwins. Real-time investigations on the formation of $\text{Cu}(\text{In},\text{Ga})\text{Se}_2$ while annealing precursors produced with a combination of sputtering and thermal evaporation.- *Materials Research*

- Society Symposium Proceedings 1012: Materials Research Society, 2007, 1012-Y10-01
73. S. Jost, F. Hergert, R. Hock, J. Schulze, A. Kirbs, T. Voss, M. Purwins, M. Schmid. Real - time investigations on the formation of CuInSe₂ film solar cell absorbers from electrodeposited precursors. - *Solar Energy Materials and Solar Cells*, 2007, 91, p. 636–644.
 74. F. Hergert, S. Jost, R. Hock, M. Purwins, J. Palm. A thermodynamical approach to the formation reactions of sodium- doped Cu(In,Ga)Se₂ . - *Thin Solid Films*, 2006, 511 – 512, p. 147 – 152.
 75. F. Hergert, S. Jost, R. Hock, M. Purwins, J. Palm. Formation reactions of chalcopyrite compounds and the role of sodium doping. - *Thin Solid Films*, 2007, 515, p. 5843– 5847.
 76. F. Hergert, S. Jost, R. Hock, M. Purwins, J. Palm. Predicted reaction paths for the formation of multinary chalcopyrite compounds. - *physica status solidi (a)*, 2006, 203, p. 2615-2623.
 77. B. Barcones, A. Perez-Rodriguez, L. Calvo-Barrio, A. Romano-Rodriguez, J.R. Morante, E. Rudigier, I. Luck, J. Djordjevic, R. Scheer. In situ and ex situ characterisation of thermally induced crystallization of CuInS₂ thin films for solar cell. - *Thin Solid Films*, 2005, 480–481, p. 362–366.
 78. Ch. von Klopmann, J. Djordjevic, E. Rudigier, R. Scheer. Real-time studies of phase transformations in Cu-In-Se-S thin films 2. Sulfurization of Cu-In precursors. - *Journal of Crystal Growth*, 2006, 289 , p.121–133.
 79. J. Djordjevic, E. Rudigier, R. Scheer. Real-time studies of phase transformations in Cu-In-Se-S thin films – 3: Selenization of Cu-In precursors.- *Journal of Crystal Growth*, 2006, 294, p. 218–230.
 80. A. Joswig, M. Gossila, H. Metzner, U. Reislöhner, Th. Hahn, W. Witthuhn. Sulphurization of single-phase Cu₁₁In₉ precursors for CuInS₂ solar cells. - *Thin Solid Films*, 2007, 515, p. 5921–5924.
 81. R. Caballero, S. Siebentritt, K. Sakurai, C. A. Kaufmann, H.-W. Schock, M.Ch. Lux-Steiner. Effect of Cu excess on three – stage CuGaSe₂ thin films using in-situ process controls. - *Thin Solid Films*, 2007, 515, p. 5862–5866.
 82. I. M. Kötschau, H. Rodriguez-Alvarez, C. Streeck, A. Weber, M. Klaus, I. Asmus Denks, J. Gibmeier, Ch. Genzel, and H.-W. Schock. Pressure dependent rapid thermal processing of CuInS₂ thin films investigated by in-situ energy dispersive X-ray diffraction. - *Materials Research Society Symposium Proceedings 1012: Materials Research Society*, 2007,1012-Y13-09
 83. K. Jimbo, S. Yamada, T. Kamimura, W. S. Maw, H. Katagiri, T. Fukano, T. Ito, T. Motohiro. Characterization of Cu₂ZnSnS₄ thin films prepared by co-sputtering and sulfurization technique. 22nd European Photovoltaic Solar Energy Conference, 2007, Milan, Italy, p. 2373-2376.
 84. A. Weber, I. Kötschau, S. Schorr, H.-W. Schock. Formation of Cu₂ZnSnS₄ and Cu₂ZnSnS₄-CuInS₂ thin films investigated by in-situ energy dispersive X-ray diffraction. - *Materials Research Society Symposium Proceedings 1012: Materials Research Society*, 2007, 1012-Y03-35

85. S. Jost, F. Hergert, R. Hock, J. Schulze, A. Kirbs, T. Voss, M. Purwins. The formation of CuInSe_2 thin film solar cell absorbers from electroplated precursors with varying selenium content. - *Solar Energy Materials and Solar Cells*, 2007, 91, p. 1669-1675.
86. S. Jost, F. Hergert, R. Hock, T. Voss, J. Schulze, A. Kirbs, M. Purwins, V. Probst, J. Palm. The formation of $\text{CuIn}(\text{S},\text{Se})_2$ thin film solar cell absorbers from electroplated precursors. - *Materials Research Society Symposium Proceedings 1012: Materials Research Society*, 2007, 1012-Y03-29
87. S. Jost, R. Schurr, F. Hergert, R. Hock, J. Schulze, A. Kirbs, T. Voss, M. Purwins, J. Palm, I. Mys. The formation of CuInSe_2 thin-film solar cell absorbers by laser annealing of electrodeposited precursors. - *Solar Energy Materials and Solar Cells*, 2008, 92, p. 410-417
88. N. Stratieva, E. Tzvetkova, M. Ganchev, K. Kochev, I. Tomov. Structural and optical properties of electrodeposited CuInSe_2 layers. - *Solar Energy Materials and Solar Cells*, 1997, 45, p. 87-96.
89. C. Guillen, J. Herrero. Improvement of the optical properties of electrodeposited CuInSe_2 thin films by thermal and chemical treatments. - *Solar Energy Materials and Solar Cells*, 1996, 43, p. 47-57.
90. J. L. Xu, X.F. Yao, J.Y. Feng. The influence of the vacuum annealing process on electrodeposited CuInSe_2 films. - *Solar Energy Materials and Solar Cells*, 2002, 73, p. 203-208.
91. L. Zhang, F.D. Jiang, J.Y. Feng. Formation of CuInSe_2 and $\text{Cu}(\text{In},\text{Ga})\text{Se}_2$ films by electrodeposition and vacuum annealing treatment. - *Solar Energy Materials and Solar Cells*, 2003, 80, p. 483-490.
92. S. H. Kang, Y.-K. Kim, D.-S. Choi, Y.-E. Sung. Characterization of electrodeposited CuInSe_2 (CIS) film. - *Electrochimica Acta*, 2006, 51, p. 4433-4438.
93. R. Friedfeld, R. P. Raffaele, J.G. Mantovani. Electrodeposition of $\text{CuIn}_x\text{Ga}_{1-x}\text{Se}_2$ thin films. - *Solar Energy Materials and Solar Cells*, 1999, 58, p. 375-385.
94. K. Bouabid, A. Ihlal, A. Manar, A. Outzourhit, E.L. Ameziane. Effect of deposition and annealing parameters on the properties of electrodeposited $\text{CuIn}_{1-x}\text{Ga}_x\text{Se}_2$ thin films. - *Thin Solid Films*, 2005, 488, p. 62-67.
95. M. E. Calixto, P. J. Sebastian. Depth profile analysis of CuInSe_2 (CIS) thin films grown by electrodeposition technique. - *Solar Energy Materials and Solar Cells*, 2000, 63, p. 335-345.
96. J.-F. Guillemoles., A. Lusson, P. Cowache, S. Massaccesi, J. Vedel, D. Lincot. Recrystallization of electrodeposited copper indium diselenide thin films in an atmosphere of elemental selenium. - *Advanced Materials*, 1994, p. 376-379.
97. C. Sene, M. Estela Calixto, Kevin D. Dobson, Robert W. Birkmire. Electrodeposition of CuInSe_2 absorber layers from pH buffered and non-buffered sulfate-based solutions.- *Thin Solid Films*, 2008, 516, p. 2188-2194
98. P.J Sebastian, S.A. Gamboa, M.E. Calixto, H.Nguyen-Cong. Poly-3-methylthiophene/ CuInSe_2 solar cell formed by electrodeposition and

- processing. - *Semiconductor Science and Technology*, 1998, 13, p. 1459-1462
99. D. D. Shivagan, P. J. Dale, A. P. Smantilleke, L. M. Peter. Electrodeposition of chalcopyrite films from ionic liquid electrolytes.- *Thin Solid Films*, 2007, 515, p. 5899-5903.
 100. M. E. Calixto, K. D. Dobson, B. McCanless, R. W. Brikmire. Single bath electrodeposition of CuInSe₂ and Cu(In,Ga)Se₂ for thin film photovoltaic cells. - *Proceedings of 31st IEEE Photovoltaic Specialist Conference: Lake Buena Vista, USA, 2005*, p. 378-381.
 101. S. Moorthy Babu, A. Ennaoui, M.Ch. Lux-Steiner. Compositional and growth procedure-dependent properties of electrodeposition CuInSe₂ thin film. - *Journal of Crystal Growth*, 2005, 275, p. 1241-1246.
 102. R. P. Wijesundera, W. Siripala. Preparation of CuInS₂ thin films by electrodeposition and sulphurisation for applications in solar cells. - *Solar Energy Materials and Solar Cells*, 2004, 81, p. 147-154.
 103. M. Ganchev, J. Kois, M. Kaelin, S. Bereznev, E. Tzvetkova, O. Volobujeva, N. Stratieva, A. Tiwari. Preparation of Cu(In,Ga)Se₂ layers by selenization of electrodeposited Cu-In-Ga precursors. - *Thin Solid Films*, 2006, 511 – 51, p. 325 – 327.
 104. JCPDS Powder Diffraction Cards, Joint Committee on Powder Diffraction Standards, Swarthmore PA
 105. G. Morell, R.S. Katiyar, S.Z. Weisz, T. Walter, H.-W. Schock, I. Balberg. Crystalline phases at the p- to n-type transitions in Cu-ternary semiconducting films. - *Applied Physics Letters*, 1996, 69, p. 987-989.
 106. D. Papadimitrou, N. Esser, C. Xue. Structural properties of chalcopyrite thin films studied by Raman spectroscopy. - *physica status solidi (b)*, 2005, 242, p. 2633-2643.
 107. O.A. Balitskii, V.P. Savchyn, V.O. Yukhymchuk. Raman investigation of InSe and GaSe single crystals oxidation. - *Semiconductor Science and Technology*, 2002, 17, L1-L4.
 108. A. Antony, A.S. Asha, R. Yoosuf, R. Manoj, M.K. Jayaraj. Growth of CuInS₂ thin films by sulphurization of Cu-In. - *Solar Energy Materials and Solar Cells*, 2004, 81, p. 407-417.
 109. H. Choi, D. H. Lee. Preparation of CuIn_{1-x}Ga_xSe₂ films by metalorganic chemical vapour deposition using three precursors. - *Thin Solid Films*, 2007, 515, p. 4778-4782.
 110. J. Alvarez-Garcia, E. Rudiger, N. Rega, B. Barcones, R. Scheer, A. Perez-Rodriguez, J. R. Morante. Growth process monitoring and quality assessment of CuInS(Se)₂ based solar cells by Raman spectroscopy. - *Thin Solid Films*, 2003, 431-432, p. 122-125.
 111. D. Abou-Ras, S. Schorr, H.W. Schock. Grain-size distributions and grain boundaries of chalcopyrite-type thin films. - *Journal of Applied Crystallography*, 2007, 40, p. 841-848.
 112. H. Mouninho, R. Dhere, C-S. Jiang, B. To, M. Al-Jassim. Electron-Backscatter Diffraction of Photovoltaic Thin Films. - *Materials Research*

- Society Symposium Proceedings 1012: Materials Research Society, 2007, 1012-Y12-04.
113. A. Feltrin, A. Freindlich. Material considerations for terawatt level deployment of photovoltaics. - *Renewable Energy*, 2008, 33, p. 180-185.
 114. R.A. Wibowo, E.S. Lee, B. Munir, K. H.Kim. Pulsed laser deposition of quaternary $\text{Cu}_2\text{ZnSnSe}_4$ thin films. - *physica status solidi (a)*, 2007, 204, p. 3373-3379.
 115. K. Moriya, K. Tanaka, H. Uchiki. $\text{Cu}_2\text{ZnSnS}_4$ thin films annealed in H_2S atmosphere for solar cell absorber prepared by pulsed laser deposition. - *Japanese Journal of Applied Physics*, 2008, 47, p. 602-604.
 116. R. A. Wibowo, W. S. Kim, E. S. Lee, B. Munir, K.H. Kim. Single step preparation of quaternary $\text{Cu}_2\text{ZnSnSe}_4$ thin films by RF magnetron sputtering from binary chalcogenide targets. - *Journal of Physics and Chemistry of Solids*, 2007, 68, p. 1908-1913.
 117. J.-S. Seol, S.-Y. Lee, J.-C. Lee, H.-D. Nam, K.-H. Kim. Electrical and optical properties of $\text{Cu}_2\text{ZnSnS}_4$ thin films prepared by rf magnetron sputtering process. - *Solar Energy Materials and Solar Cells*, 2003, 75, p. 155-162.
 118. K. Jimbo, R. Kimura, T. Kamimura, S. Yamada, W. S. Maw, H. Araki, K. Oishi, H. Katagiri. $\text{Cu}_2\text{ZnSnS}_4$ -type thin film solar cells using abundant materials. - *Thin solid films*, 2007, 515, p. 5997-5999.
 119. T. Tanaka, D. Kawasaki, M. Nishio, Q. Guo, H. Ogawa. Fabrication of $\text{Cu}_2\text{ZnSnS}_4$ thin films by co-evaporation. - *physica status solidi (c)*, 2006, 3, p. 2844-2847.
 120. H. Katagiri. $\text{Cu}_2\text{ZnSnS}_4$ thin film solar cells. - *Thin Solid Films*, 2005, 480-481, p. 426-432.
 121. N. Kamoun, H. Bouzouita, B. Rezig. Fabrication and characterization of $\text{Cu}_2\text{ZnSnS}_4$ thin films deposited by spray pyrolysis technique. - *Thin Solid Films*, 2007, 515, p.5949-5952.
 122. K. Ramanathan, M. A. Contreras, C.L. Perkins, S. Asher, F.S. Hasoon, J. Keane, D. Young, M. Romero, W. Metzger, R. Noufi, A. Duda. Properties of 19.2% efficiency ZnO/CdSCuInGaSe_2 thin film solar cells. - *Progress in Photovoltaics: Research and Applications*, 2003, 11, p. 225-230.
 123. M. Altosaar, J. Raudoja, K. Timmo, M. Danilson, M. Grossberg, J. Krustok, E. Mellikov. $\text{Cu}_2\text{Zn}_{1-x}\text{Cd}_x\text{Sn}(\text{Se}_{1-y}\text{S}_y)_4$ solid solutions as absorber materials for solar cells, *physica status solidi (a)*, 2008, 205, p. 167-170.
 124. R. A. Wibowo, W. S. Kim, B. Munir, K. H. Kim. Growth and Properties of Stannite-Quaternary $\text{Cu}_2\text{ZnSnSe}_4$ Thin Films Prepared by Selenization of Sputtered Binary Compound Precursors. - *Advanced Materials Research*, 2007, 29-30, p. 79-82.
 125. G. Licovsky, J. Mikkelsen, W. Y. Liang, R. M. White, R. M. Martin. Optical Phonon Anisotropies in the Layer Crystals SnS_2 and SnSe_2 - *Physical Review*, 1976, B 14, p. 1663-1668.
 126. S. Venkatachalam, S. Agilan, D. Mangalaraj, Sa.K. Narayandass. Optoelectronic properties of ZnSe thin films. - *Materials Science in Semiconductor Processing*, 2007, 10, p. 128-132.

127. R. Takei, H. Tanino, S. Chichibuc, H. Nakanishi. Depth profiles of spatially-resolved Raman spectra of a CuInSe₂-based thin-film solar cell. - Journal of Applied Physics, 1996, 79, p. 2793-2975.

ABSTRACT

This study focuses on the influence of different post-treatments on the structure, morphology and composition of different alloy and stacked metallic CuInSe_2 and $\text{Cu}_2\text{ZnSnSe}_4$ layers and electrodeposited CuInSe_2 layers. It is shown that Co-sputtering of Cu-In layers leads to rough layers with a bi-layer structure of the surface in which island-type CuIn_2 crystals are formed in a small-crystalline copper-rich $\text{Cu}_{11}\text{In}_9$ matrix layer. The diffusion Cu from the bulk of the layer to the surface at lower temperatures (up to 300°C) leads to the formation of different binary copper selenides. The selenization of In proceeds at higher temperatures and CuInSe_2 formation is described as a reaction of different binary selenides. The combination of Raman, EDX and EBSD studies allows us to show that CuInSe_2 films formed at temperatures higher than 420°C are homogeneous and in single-phase composition with a preferred orientation of crystals along the (112) plane. The composition of films corresponds to the composition of precursor sputtering targets. The importance of twin crystal formation in the formed CuInSe_2 layers as the strain compensation mechanism is determined. MoSe_2 layer was formed only consequent to the formation of CuInSe_2 phase and no separate binary phases were found in the selenized layers.

The stacked Sn-Zn-Cu films with a different sequence of composing metals were prepared by vacuum evaporation and selenized in the elemental Se atmosphere. The structure of precursor films depends on the sequence of layers. It is shown that the pathway to form the $\text{Cu}_2\text{ZnSnSe}_4$ phase under the pressure of elemental Se and the phase composition of selenized films depend on the temperature of selenization. Selenization begins with the formation of binary Cu-selenides, with the composition varying with the temperature of selenization. The selenization of Sn-Zn-Cu films at temperatures higher than 375°C results always in multiphase films that consist of high quality $\text{Cu}_2\text{ZnSnSe}_4$ crystals with a size of about $2\ \mu\text{m}$ and of a separate phase of ZnSe. The formation of MoSe_2 layer was detected at selenization temperatures higher than 400°C .

It was found that the recrystallization processes in one-step electrodeposited CuInSe_2 thin films are dependent on Se vapour pressure and precursor film composition. For samples annealed in Se vapour at 450°C , the recrystallization of chalcogenide CuInSe_2 occurs rapidly with the segregation of Cu-Se phases onto the bottom of CIS films and the formation of CIS grains different by size and composition. The diffusion of elements in the CIS film matrix and the segregation of localized structures are slower in the process of vacuum annealing than in the selenization process. The formation of MoSe_2 interlayer was observed only in samples thermally treated in selenium atmosphere.

KOKKUVÕTE

Käesoleva töö eesmärgiks oli komplekselt uurida erinevate järeltötluste mõju nii Cu-In sulami, kihiliste Cu-Zn-Sn õhukeste kihtide kui ka elektrokeemiliselt sadestatud CuInSe₂ kilede struktuurile, pinnamorfoloogiale ja koostisele.

Läbiviidud uuringud on näidanud, et Cu ja In üheaegne pihustamine annab tulemuseks konarliku pinnaga kihid, kus CuIn₂ kristallid moodustavad "saarekesi" peenekristallilises vaserikkas Cu₁₁In₉ aluskihis. Saadud kihtide edasisel madalatemperatuurisel seleniseerimisel (kuni 300°C) Se atmosfääris difundeerub vask pinnale moodustades erinevaid vaskseleniide. Kõrgematel temperatuuridel seleniseerub indium ja CuInSe₂ moodustumise aluseks ongi reaktsioon eelnevalt moodustunud binaarsete seleniidide vahel. Erinevate urimismeetodite nagu Raman, EDX ja EBSD kasutamisel saadud tulemused on võimaldanud näidata, et seleniseerimine kõrgematel temperatuuridel kui 420°C viib homogeensete ühefaasiliste CuInSe₂ kilede tekkele, mille koostis vastab Cu-In lähtesulami koostisele. On näidatud et CuInSe₂ kilede moodustumisprotsessis tomub intensiivne kaksikkristallide teke, mis aitab kompenseerida CuInSe₂ kilede moodustumisel toimunud mahu suurenemisest tekkinud mehhaanilisi pingeid. Mo seleniseerimine ja MoSe₂ teke algab temperatuuridel kõrgemad kui 400°C ja alles pärast seda, kui kogu CuInSe₂ moodustumisprotsess on lõppenud.

Erineva metallikihtide järjestusega Sn-Zn-Cu struktuurid valmistati vaakuum-aurustuse meetodil. Kihiliste struktuuride morfoloogia sõltus metallikihtide järjestusest lähtekiles. On näidatud, et Cu₂ZnSnSe₄ moodustumise mehhanism ja saadavate kilede koostis sõltub selenisatsiooni temperatuurist. Seleniseerimine algab erinevate temperatuurist sõltuva koostisega vaskseleniidide moodustumisega kihtide pinnal. Alles seleniseerimine temperatuuridel kõrgemad kui 375°C viib mitmefaasiliste kilede tekkele, kus lisaks domineerivale Cu₂ZnSnSe₄ faasile esineb eraldi ZnSe lisandfaas. Analoogiliselt Cu-In seleniseerimisega algab Sn-Zn-Cu struktuuride seleniseerimine vaskseleniidide moodustumisega kihtide pinnal. Seleniseerimine temperatuuridel üle 375°C viib Cu₂ZnSnSe₄ moodutumisele ja mitmefaasiliste kilede tekkele, kus lisaks domineerivale Cu₂ZnSnSe₄ faasile esineb eraldi ZnSe lisandfaas.

Antud uurimistöö käigus on näidatud, et elektrokeemiliselt sadestatud CuInSe₂ õhukeste kilede rekristallisatsioon sõltub termilistest tötlustest ja keskkonnast. Temperatuuridel üle 450°C toimub intensiivne Cu-Se faaside segregatsioon kilede alumisse ossa. Segregatsiooniprotsess on tundavamalt intensiivsem Se atmosfääris kui tötlustel vakuumis. MoSe₂ moodustumist täheldati vaid kilede tötlustel Se keskkonnas.

APPENDIX A

